




Endothelial cell-derived extracellular vesicles expressing surface VCAM1 promote sepsis-related acute lung injury by targeting and reprogramming monocytes

Lu Wang¹  | Ying Tang¹  | Jiajian Tang¹ | Xu Liu¹ | Shuangfeng Zi¹ | Songli Li¹ | Hanbing Chen¹ | Airan Liu¹ | Wei Huang¹ | Jianfeng Xie¹ | Ling Liu¹ | Jie Chao^{1,2} | Haibo Qiu¹ 

¹Jiangsu Provincial Key Laboratory of Critical Care Medicine, Department of Critical Care Medicine, Zhongda Hospital, School of Medicine, Southeast University, Nanjing, China

²Department of Physiology, School of Medicine, Southeast University, Nanjing, China

Correspondence

Haibo Qiu and Jie Chao, Jiangsu Provincial Key Laboratory of Critical Care Medicine, Department of Critical Care Medicine, Zhongda Hospital, School of Medicine, Southeast University, Nanjing 210009, China.
Email: haiboq2000@163.com; chaojie@seu.edu.cn

Funding information

National Natural Science Foundation of China, Grant/Award Numbers: 81930058, 82341032, 82072154; The National Key R&D Program of China, Grant/Award Numbers: 2022YFC2504403, 2021YFC2500804; The Jiangsu Provincial Key Medical Discipline (Laboratory), Grant/Award Number: ZDXKA2016025; The Jiangsu Provincial Special Program of Medical Science, Grant/Award Number: BE2019749

Abstract

Acute lung injury (ALI)/acute respiratory distress syndrome (ARDS) is a common life-threatening syndrome with no effective pharmacotherapy. Sepsis-related ARDS is the main type of ARDS and is more fatal than other types. Extracellular vesicles (EVs) are considered novel mediators in the development of inflammatory diseases. Our previous research suggested that endothelial cell-derived EVs (EC-EVs) play a crucial role in ALI/ARDS development, but the mechanism remains largely unknown. Here, we demonstrated that the number of circulating EC-EVs was increased in sepsis, exacerbating lung injury by targeting monocytes and reprogramming them towards proinflammatory macrophages. Bioinformatics analysis and further mechanistic studies revealed that vascular cell adhesion molecule 1 (VCAM1), overexpressed on EC-EVs during sepsis, activated the NF- κ B pathway by interacting with integrin subunit alpha 4 (ITGA4) on the monocyte surface, rather than the tissue resident macrophage surface, thereby regulating monocyte differentiation. This effect could be attenuated by decreasing VCAM1 levels in EC-EVs or blocking ITGA4 on monocytes. Furthermore, the number of VCAM1⁺ EC-EVs was significantly increased in patients with sepsis-related ARDS. These findings not only shed light on a previously unidentified mechanism underlying sepsis-related ALI/ARDS, but also provide potential novel targets and strategies for its precise treatment.

KEYWORDS

ALI/ARDS, endothelial cell, extracellular vesicle, monocyte, sepsis

1 | INTRODUCTION

Acute lung injury (ALI)/acute respiratory distress syndrome (ARDS) is a common respiratory critical syndrome caused by direct pulmonary insults (e.g., pneumonia, aspiration) or non-pulmonary insults (e.g., sepsis, trauma), with a mortality rate ranging from 35% to 46% (Fan et al., 2018). Sepsis-related ARDS is the main type of ARDS and is more fatal than other types (Gorman et al., 2022). The essence of ARDS is an overwhelming and uncontrolled inflammatory reaction, characterized by the massive infiltration of inflammatory cells, the formation of cytokine storms, increased permeability of pulmonary capillaries and pulmonary oedema (Matthay et al., 2019). Although progress has been made in understanding the pathogenesis of ARDS since

Lu Wang and Ying Tang contributed equally to the paper.

This is an open access article under the terms of the [Creative Commons Attribution-NonCommercial-NoDerivs License](https://creativecommons.org/licenses/by-nc-nd/4.0/), which permits use and distribution in any medium, provided the original work is properly cited, the use is non-commercial and no modifications or adaptations are made.

© 2024 The Authors. *Journal of Extracellular Vesicles* published by Wiley Periodicals LLC on behalf of International Society for Extracellular Vesicles.

its first report in 1967, the current treatment of ARDS mainly relies on supportive care with mechanical ventilation and lacks specific and effective pharmacotherapy (Shaw et al., 2019). These treatments cannot fundamentally block disease progression and improve the prognosis of patients. Hence, there is an urgent need to explore new targets to inhibit the amplification of the inflammatory cascade.

The monocyte-macrophage system plays a central role in the initiation and progression of ALI/ARDS (Thompson et al., 2017). An imbalance between proinflammatory (M1 type) and anti-inflammatory (M2 type) macrophages is one of the main causes of ARDS, in which M1 macrophages act as a proinflammatory phenotype and can promote the occurrence of ARDS. Based on their origins, macrophages can be classified into tissue resident macrophages (TR-M ϕ s) and monocyte-derived macrophages (Mo-M ϕ s). When an infection occurs, classical Ly6C^{high} monocytes migrate into the lung and differentiate into Mo-M ϕ s to replace TR-M ϕ s (Mass et al., 2023; Park et al., 2022). Most previous studies have analysed the two together, considering that they perform the same function in the disease. However, an increasing number of recent studies have demonstrated unexpected functional heterogeneity between the two (Li et al., 2022). In ARDS caused by SARS-CoV-2 infection, Mo-M ϕ s drive the inflammatory response and undergo more significant reprogramming than TR-M ϕ s, in which the cell phenotype is altered due to transcriptomic changes (Bohnacker et al., 2022; Lee et al., 2021). In a murine model of *Pseudomonas aeruginosa*-induced ALI, Mo-M ϕ s have higher expression of M1 macrophage markers (CD86, MHCII and iNOS) compared to other cell populations (including TR-M ϕ s) in the lung (Xu et al., 2020). Animal experiments have shown that depletion of peripheral blood monocytes can reduce ALI (Dhaliwal et al., 2012). These findings strongly suggest that Mo-M ϕ s play a crucial role in ARDS. In pulmonary ARDS, the recruitment and differentiation of monocytes are mainly mediated by the chemokines release from cells in alveoli activated by pathogen-associated molecular patterns (PAMPs) or damage-associated molecular patterns (DAMPs). However, in non-pulmonary sepsis-related ARDS, the mechanism by which monocytes migrate from peripheral circulation into the lung and differentiate into macrophages in the absence of PAMPs and DAMPs in the alveoli remains largely unexplored. Exploring factors that mediate monocyte migration and differentiation, and the differential changes between Mo-M ϕ s and TR-M ϕ s will provide promising strategies to treat sepsis-related ALI/ARDS.

Recently, emerging evidence suggests that extracellular vesicles (EVs) are involved in regulating immune cell function and mediating the development of various inflammatory diseases (Grange & Bussolati, 2022; Yates et al., 2022). EVs are lipid bilayer-enclosed vesicles that can be released by almost all cell types under normal and pathological conditions, and they can function in long-distance intercellular communication with good stability and a long duration of action (van Niel et al., 2018). It has been reported that EVs mediate the recruitment and differentiation of monocytes in hepatic diseases (Guo et al., 2019; Hou et al., 2020) and play a role in the development of ARDS (Hu et al., 2022). Studies have shown a significant increase in the amount of endothelial cell-derived extracellular vesicles (EC-EVs) in the circulation of patients with ARDS compared to healthy subjects (Cheng et al., 2017). Our earlier research using an *ex vivo* perfused human lung model revealed that EVs in the perfusate of the *E. coli*-induced *ex vivo* human ALI model were mainly derived from endothelial cells; injection of these EVs into naïve human lungs resulted in ALI, and ALI was reduced after blocking the uptake of EVs (Liu et al., 2019). Thus, we hypothesize that EC-EVs regulate the recruitment and differentiation of monocytes in sepsis-related ARDS, thereby playing an important role in the development of the disease. Validating this hypothesis and exploring the underlying mechanisms will provide new targets for the precision treatment of sepsis-associated ALI/ARDS.

2 | MATERIALS AND METHODS

2.1 | Isolation of EVs

To isolate EVs from cell culture supernatant, medium was firstly centrifuged for 5 min at $300 \times g$ to remove cells. Subsequently, the supernatant was centrifuged at $2000 \times g$ for 20 min to remove cell debris and further centrifuged at $13,000 \times g$ for 30 min to remove pellet containing large EVs. The resulting supernatant was ultracentrifuged at $200,000 \times g$ for 90 min to pellet all EVs. The pellet was washed with sterile PBS followed by another centrifugation step at $200,000 \times g$ to purify EVs (Figure S1a).

To isolate plasma EVs, peripheral blood samples were anticoagulated with EDTA and then centrifuged at $1000 \times g$ for 15 min at 4°C to remove red blood cells, white blood cells and platelets. The supernatant was plasma and centrifuged at $2000 \times g$ for 20 min to remove cell debris, and the subsequent serial centrifugation steps were the same as those for cell culture supernatant. All centrifugation steps were performed at 4°C .

It should be added that EVs produced by normal endothelial cells were referred to as 'N-EC-EVs', while EVs produced by endothelial cells stimulated with LPS were referred to as 'L-EC-EVs'. L-EC-EVs with low VCAM1 expression (VCAM1-KD L-EC-EVs) were obtained from VCAM1-knockdown endothelial cell line (the construction method is described in the Supplementary) with LPS stimulation, and the negative control L-EC-EVs (NC L-EC-EVs) were obtained from the negative control endothelial cell line upon LPS stimulation. Cell culture conditions are detailed in the supplementary methods.

2.2 | Characterization of EVs

The morphology of EVs was examined by a JEM-2100 transmission electron microscope (TEM, Tokyo, Japan). The size distribution and particle concentration were detected by a nanoparticle tracking analyser (Particle Metrix ZetaView, Meerbusch, Germany). The levels of protein markers of purified EVs (Alix, CD63, and CD9) and a negative marker (GM130) were verified by western blotting. The protein concentration of EVs was quantified using a bicinchoninic acid (BCA) protein assay kit (Beyotime, Shanghai, China) according to the manufacturer's protocol. The amount of VCAM1 on the surface of EVs was determined by the mouse VCAM1 Quantikine ELISA Kit (Proteintech, Wuhan, China) or western blotting, and the percentage of VCAM1⁺ EVs was determined by nanoflow cytometry.

2.3 | EV analysis by nanoflow cytometry

The Flow NanoAnalyzer N30E (NanoFCM Inc., China) was used to detect the surface protein marker of EVs. The following antibodies were used: FITC-conjugated rat anti-mouse CD31 (102406, BioLegend), APC-conjugated mouse anti-mouse VCAM1 antibody (105718, BioLegend), FITC-conjugated mouse anti-human CD31 antibody (557508, BD), and APC-conjugated mouse anti-human VCAM1 antibody (305809, BioLegend). Equal amounts of EV samples were incubated with the recommended dose of antibody at 37°C for 30 min. Then, the mixture was washed with PBS and centrifuged at 120,000 × *g* for 90 min at 4°C. The pellet was washed once and resuspended in 100 μL of PBS for phenotype analysis.

2.4 | Human samples

Blood samples were obtained from patients who admitted in the Department of Critical Care Medicine, Zhongda Hospital, Southeast University, Nanjing, China. Non-pulmonary sepsis induced ARDS patients who met the criteria of Sepsis 3.0 (Singer et al., 2016) and Berlin definition (Ranieri et al., 2012) within 24 h were included in the study. Exclusion criteria were as follows: (1) under 18 years old; (2) patients with cancer, severe immunocompromise, pregnancy, or lactation. Critically ill patients without ARDS or sepsis and met the above exclude criteria were included as the patient control. A group of healthy volunteers were also enrolled as normal control. Peripheral blood samples were collected in EDTA-K2-coated anti-coagulant tubes. All procedures were conducted under the approval of the Independent Ethics Committee for Clinical Research of Zhongda Hospital, Southeast University (approval number: 2019ZDSYLL218-P01), and informed consent was obtained from all subjects prior to sample collection.

2.5 | Animal experiments

Wild-type C57BL/6J mice (male, 7–8 weeks old) were purchased from GemPharmatech (Nanjing, China). All animal studies conformed to the National Institutes of Health Guidelines on the Use of Laboratory Animals and were approved by the Institutional Animal Care and Use Committee of the medical school, Southeast University (Approval number: 20190222014).

To induce sepsis-induced ALI, mice were subjected to caecal ligation and puncture (CLP) surgery as previously described (Rittirsch et al., 2009). The detailed methods are provided in the Supplementary information.

To study the effects of EC-EVs, mice were injected intravenously with N-EC-EVs/L-EC-EVs (1×10^{10} particles/mouse). An equal volume of PBS was used as the negative control. Mice were sacrificed 24 h later to assess lung inflammation and injury. To investigate the cellular localization of EC-EVs in the lung, DiD-labelled EVs were injected intravenously into mice. At 1 h after injection, the blood of the mice was collected, and lung tissues were taken after perfusion with PBS. To deplete monocytes, mice were injected with clodronate liposomes (Clo-lip, 7 mg/mL, 200 μL/mouse) (FormuMax, USA) via the tail vein 24 h before and 3 h after EV treatment. To deplete TR-Mφs, Clo-lip (100 μL/mouse) were administered via intratracheal injection 24 h before EV treatment. Mice in the control group were administered the same volume of control liposomes (Con-lip). Mice were euthanized at 24 h after EV treatment, and lung tissues and blood were collected for further analysis. To detect the role of integrin subunit alpha 4 (ITGA4) in mediating monocyte differentiation, mice were injected intravenously with either an anti-ITGA4 blocking antibody (553153, BD) or an IgG isotype control (556968, BD) at a dose of 2 mg/kg body weight 4 h before EV treatment, and lung tissues were collected 24 h later for further analysis. Methods of lung histopathologic analysis and lung wet/dry weight ratio measurement are described in the supplementary methods.

2.6 | Distribution of EVs in different tissues

To assess the *in vivo* tissue distribution of L-EC-EVs, mice were intravenously injected with DiD-labelled L-EC-EVs (1×10^{10} particles/mouse) or an equal volume of PBS. At different time points after injection, the major tissues, including the heart, lung, liver, kidney, and spleen, were collected after sacrificing the mice. *Ex vivo* fluorescence imaging was conducted using the IVIS Spectrum imaging system (PerkinElmer, USA). The method of labelling EVs with DiD is described in the Supplementary.

2.7 | Monocyte isolation and treatment

Monocytes were isolated from the tibias and femurs of C57BL/6J mice by negative selection using an EasySep Mouse Monocyte Isolation Kit (Stemcell Technologies, Canada) following the manufacturer's procedures. The cells were cultured in RPMI 1640 (Gibco, USA) supplemented with 10% heat-inactivated FBS, and 1% penicillin-streptomycin. Cells were plated in a 12-well plate (5×10^5 cells/well) and rested for 1 h prior to the experiments. They were then treated with N-EC-EVs or L-EC-EVs (10^9 particles/well) for 24 h, and the culture medium was collected for cytokine analysis. Moreover, the cells were used to extract total RNA and stained with fluorochrome-conjugated antibodies to clarify the effects of EVs on their phenotype and function. For experiments using inhibitors, cells were pretreated with the NF- κ B inhibitor Bay11-7082 (10 μ M, MCE, USA) for 30 min before adding EVs. To detect the role of ITGA4 in mediating monocyte differentiation, cells were pretreated with an anti-ITGA4 blocking antibody or an IgG isotype control (10 μ g/ 5×10^5 cells) for 1 h and then incubated with PBS/L-EC-EVs for 24 h. Both cells and culture medium were collected for further analysis.

2.8 | Isolation of pulmonary TR-M ϕ s

Alveolar macrophages (AMs) are TR-M ϕ s within lung tissues during resting-state, which reside on the epithelial surface of alveoli and are easily obtained by bronchoalveolar lavage (Ginhoux & Guillemins, 2016; Lazarov et al., 2023; Mass et al., 2023). Hence, we obtained pulmonary TR-M ϕ s by bronchoalveolar lavage from healthy mice as previously described (Baasch et al., 2021). Briefly, after euthanasia, the tracheas of mice were exposed via a median neck incision, and PBS with EDTA (2 mM) was injected into the lungs through a 20-gauge catheter attached to a 1 mL syringe. The lavage was repeated three times, and the lavage fluid from several mice was pooled. Cells were obtained by centrifugation at $300 \times g$ for 5 min at room temperature and resuspended in RPMI 1640 (Gibco, USA) supplemented with 10% heat-inactivated FBS, and 1% penicillin-streptomycin. After 2 h, nonadherent cells were removed by washing with sterile PBS, and adherent cells were treated with N-EC-EVs or L-EC-EVs for 24 h.

2.9 | In vitro uptake of EVs by monocytes

Monocytes were seeded in 96-well plates precoated with poly-L-ornithine solution (Sigma, USA), and incubated with equal amounts of PKH-67-labelled N-EC-EVs or L-EC-EVs for 12 h. An equal volume of PBS was used as a negative control. The real-time dynamic uptake process was captured every 15 min using the IncuCyte S3 Live-Cell Analysis System (Essen Bioscience, USA) and analysed by IncuCyte Software (Essen Bioscience, USA). The method of labeling EVs with PKH-67 is described in the Supplementary.

2.10 | Flow cytometry analysis

To clarify the target cell of L-EC-EVs in the lung, the lung single cell suspensions were first stained with viability dye (564406, BD) and then incubated with Fc Block (553141, BD) to reduce nonspecific binding, followed by staining with various fluorochrome-labelled antibodies: anti-CD45 (557659, BD), anti-CD11b (557396, BD), anti-Ly6G (740953, BD), anti-CD11c (117339, BioLegend), anti-F4/80 (565411, BD), anti-CD3 (557984, BD) and anti-CD19 (553786, BD). The uptake of EC-EVs in each type of cell was quantified as the mean fluorescence intensity (MFI) of DiD. To investigate the effects of EC-EVs on pulmonary macrophage differentiation, lung single cell suspensions were stained with the following fluorochrome-labelled antibodies after blocking with Fc Block: anti-CD45, anti-CD11b, anti-Ly6G, anti-F4/80, anti-CD11c, anti-CD80 (553769, BD) and anti-CD163 (155305, BioLegend). Lung single-cell suspensions were prepared as described in the Supplementary. To detect the effects of EC-EVs on monocyte and macrophage differentiation *in vitro*, cells were incubated with Fc Block and then stained with fluorochrome-conjugated antibodies against CD11b, F4/80, CD80, CD163, CD86 (742120, BD), and CD206 (141706, BioLegend). To assess the

purity of TR-M ϕ s, cells were stained with anti-CD45, CD11c and Siglec-F (562681, BD) antibodies after blocking. To detect the expression of ITGA4 on monocytes, Mo-M ϕ s and TR-M ϕ s, cells were incubated with Fc Block and then stained with an anti-ITGA4 antibody (103605/103621, BioLegend). Data were collected using the LSRFortessa X20 Flow Cytometer (BD, USA) and analysed with FlowJo_V10 software.

2.11 | RNA sequencing analysis

Monocytes were incubated with N-EC-EVs or L-EC-EVs for 24 h respectively. Then, total RNA was extracted from monocytes using TRIzol reagent (Invitrogen, USA), and transcriptome sequencing was conducted by OE Biotech Co., Ltd. (Shanghai, China). The sample quality was evaluated using a NanoDrop 2000 spectrophotometer (Thermo Scientific, USA) and Agilent 2100 Bioanalyzer (Agilent Technologies, USA). RNA-seq libraries were prepared using the VAHTS Universal V6 RNA-seq Library Prep Kit and sequenced on the Illumina NovaSeq 6000 platform. The clean reads were mapped to the mouse genome (GRCm38) using HISAT2 (Kim et al., 2015). Transcript abundance was quantified by the fragments per kilobase million (FPKM). The threshold for significantly differential expression was set at p value < 0.05 and $|\log_2FC| > 1$. The RNA-seq data generated in this study have been deposited in the Gene Expression Omnibus (GEO) under accession code GSE236215.

2.12 | Proteomic analysis of EVs

Mass spectrometry analysis of EVs was performed at EVbio Technology Co., Ltd. (Beijing, China). Samples were lysed in lysate buffer containing protease inhibitor and 8 M urea and centrifuged at $14,000 \times g$ for 20 min to collect the supernatant. After digestion and desalination, 100 μ g of protein extracted from each sample was subjected to mass spectrometry on a quadrupole Orbitrap mass spectrometer (Q Exactive HF-X, Thermo Fisher Scientific, Germany) coupled to an EASY-nLC 1200 ultrahigh-pressure system (Thermo Fisher Scientific) via a nano-electrospray ion source. Data were analysed using Proteome Discoverer 2.4 (Thermo Fisher Scientific) against the proteome database of *Mus musculus*. The proteomic data have been deposited to the ProteomeXchange Consortium via the iProX repository with the dataset identifier PXD043470.

2.13 | Statistical analysis

Statistical analysis was performed using GraphPad Prism 8.0.2 Software. Differences between two groups were assessed with a two-tailed Student's t test. One/two-way ANOVA followed by the Bonferroni post hoc test was used for multigroup (≥ 3) comparisons. Data collected at repeating time points were analysed using two-way repeated-measures ANOVA, followed by the Bonferroni post hoc test. Data are presented as the mean \pm standard error of the mean (SEM), and a p value < 0.05 was considered statistically significant.

More detailed methods (e.g., cell culture, quantitative real-time PCR (the sequences of the primers are listed in Table S1), cytokine analysis, western blot and immunofluorescence) are provided in the Supplementary information.

3 | RESULTS

3.1 | Preparation and characterization of EVs isolated from the plasma of septic mice and endothelial cells

To determine the quantitative changes in EC-EVs in the development of sepsis-related ARDS, we used nanoparticle tracking analysis (NTA) and nanoflow cytometry, and found that both the EVs concentration (Figure 1a) and the percentage of EC-EVs (Figure 1b) in the plasma of septic mice were much higher than those of sham-operated mice. To further clarify the role of EC-EVs in the development of ARDS, we isolated N-EC-EVs and L-EC-EVs from the cell culture supernatant. TEM images showed that the EVs possessed a lipid bilayer and the typical cup-shaped morphology (Figure S1b). NTA revealed that the diameters of most EVs ranged from 50 to 150 nm (Figure S1c), and endothelial cells produced more EVs after LPS stimulation (Figure S1d). Western blot analysis showed that the characteristic surface marker proteins of EVs (Alix, CD9 and CD63) were enriched in EVs, and the negative marker (GM130) was undetectable in EVs (Figure S1e). These results indicate that circulating EC-EVs are significantly increased in mice with sepsis-related ALI compared to sham-operated mice.

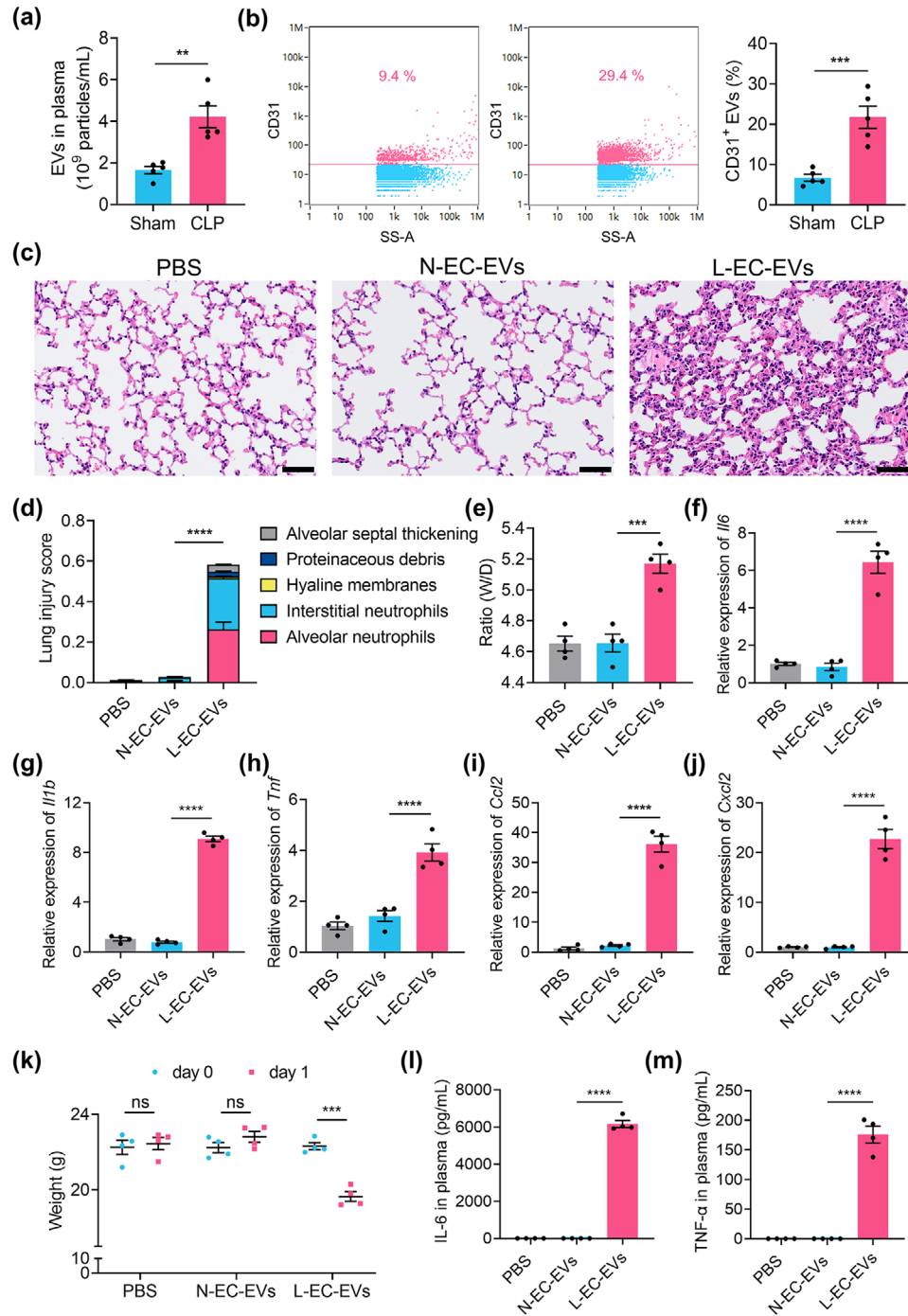


FIGURE 1 EC-EVs mediate sepsis related ALI. (a) Quantification of EVs isolated from the plasma of sham-operated and CLP mice. (b) Nanoflow cytometry analysis showing the percentage of EC-EVs in plasma EVs. (c) Mice were injected intravenously with PBS/N-EC-EVs/L-EC-EVs for 24 h, and representative histological images of H&E-stained lung sections are shown. Scale bar: 50 μ m. (d) The total lung injury score obtained from five independent histological indexes. (e) The wet/dry weight ratio of lung tissue. (f–j) Relative enrichment of proinflammatory cytokines (f–h) and chemokines (i, j) in the lung measured by qRT-PCR. (k) Changes in the body weight of mice in different groups. (l, m) Cytokine levels of IL-6 and TNF- α in the plasma of mice were quantified by ELISA. ns: not significant, ** $p < 0.01$, *** $p < 0.001$, **** $p < 0.0001$.

3.2 | L-EC-EVs can lead to ALI

To study the effects of EC-EVs released during sepsis, mice were injected intravenously with N-EC-EVs or L-EC-EVs, and lung tissues were collected 24 h later. As shown in Figure 1c, compared to mice injected with N-EC-EVs, the lung tissue of mice injected with L-EC-EVs had substantial inflammatory cell infiltration, fluid exudation and alveolar septal thickening, and thus

the lung injury score was significantly increased (Figure 1d). The ratio of lung wet-to-dry weight (Figure 1e) and the expression of proinflammatory cytokines (Figure 1f–h) and chemokines (Figure 1i, j) in lung tissues were all significantly increased in L-EC-EV-treated mice compared to control mice. These data demonstrate that L-EC-EVs can lead to ALI in mice. We also observed a significant decrease in body weight (Figure 1k) and a significant increase in plasma levels of inflammatory cytokines (Figure 1l, m) in L-EC-EV-treated mice, suggesting that L-EC-EVs can cause systemic inflammation.

3.3 | L-EC-EVs target monocytes to exacerbate ALI

The biodistribution of L-EC-EVs was tracked by intravenous injection of DiD-labelled L-EC-EVs into normal and septic mice, and the major organs were collected at different time points after injection. As shown in Figure 2a and Figure S2, the EV signal was first detected in the lung, followed by a gradual accumulation of EVs in the liver and spleen. Within 24 h, no significant EV signal was detected in the heart and kidney of normal mice. While, at 24 h after injection, the EV signal could be detected in the kidney of septic mice, which may be due to increased vascular permeability. Notably, the signal levels of L-EC-EVs in lung tissues remained relatively high and even persistently elevated in septic mice, suggesting that lung tissue was the main target organ of L-EC-EVs.

To further clarify the target cells of L-EC-EVs, DiD-labelled EC-EVs were injected into mice via the tail vein, and the blood and lung tissues of mice were collected at 1 h postinjection. By comparing the MFI of DiD in different cell types within the single-cell suspension of lung tissue after fluorescent antibody staining (Figure S3), we found that DiD-labelled L-EC-EVs were largely taken up by monocytes rather than other immune cells in the lung, and that the uptake of L-EC-EVs by pulmonary monocytes was much higher than that of N-EC-EVs (Figure 2b). In addition, the DiD MFI of monocytes in the lung tissue of the L-EC-EV-treated group was higher than that in the blood (Figure 2c), and the percentage of peripheral monocytes was significantly reduced (Figure 2d), while the percentage of monocytes in lung tissue was significantly increased (Figure 2e). These findings suggested that monocytes with a high uptake of L-EC-EVs were more prone to being recruited to or staying in the lung tissue. This phenomenon was also observed by immunofluorescence staining of lung tissue sections, where the DiD-labelled L-EC-EVs showed a high degree of colocalization with lung monocytes (Figure 2f). These data suggest that L-EC-EVs are preferentially taken up by monocytes and accumulate in the lung.

Then, the real-time dynamic uptake processes of EVs by monocytes *in vitro* were captured using a live cell imaging system. As shown in Figure 2g and Movies S1–S3, PKH67-labelled L-EC-EVs (green fluorescence) in monocytes gradually increased with increased cocubation time. Moreover, the mean intensity of green fluorescence in the L-EC-EV group was significantly higher than that in the N-EC-EV group (Figure 2h). In addition, confocal microscopy assay and Z-axis scanning confirmed that DiD-labelled L-EC-EVs (red fluorescence) could be largely internalized by monocytes (Figure 2i).

To confirm whether the proinflammatory action of L-EC-EVs occurred mainly through monocytes, we removed monocytes by intravenous injection of Clo-lip before the injection of EVs (Figure 3a). As reported previously, intravenous injection of Clo-lip could deplete virtually all circulating monocytes within 24 h, while having no effect on TR-M ϕ s in the lung (Sorkin et al., 2020). As shown in Figure S4, the intravenous administration of Clo-lip led to an approximately 90% reduction in circulating monocytes in both the N-EC-EV and L-EC-EV treated groups, confirming the effective removal of monocytes. Histological assessment of lung tissues (Figure 3b) showed reduced inflammatory cell infiltration and lung injury caused by L-EC-EVs after depletion of monocytes, and the lung injury score was significantly reduced (Figure 3c). Moreover, the mRNA levels of inflammatory cytokines (*Il6*, *Il1b*, and *Tnf*) and chemokine (*Cxcl2*) in the lung tissues of the L-EC-EV-treated group were greatly reduced after removal of monocytes (Figure 3d). In addition, flow cytometry showed a significant decrease in the proportion of neutrophils in both the lungs (Figure 3e, f) and blood (Figure 3g) of the Clo-lip+L-EC-EV group compared to the Con-lip+L-EC-EV group. The plasma levels of inflammatory cytokines (IL-6 and TNF- α) were also significantly reduced in the Clo-lip+L-EC-EV group (Figure 3h,i). Collectively, these results confirm that L-EC-EVs mediate the development of ALI by targeting monocytes.

3.4 | L-EC-EVs drive the differentiation of monocytes towards M1-type macrophages *in vitro*

To further explore the effects of EC-EVs on monocytes. The extracted primary mouse bone marrow-derived monocytes were incubated with N-EC-EVs or L-EC-EVs for 24 h. Light microscopic observation of cell morphology showed that the L-EC-EV-treated cells were enlarged and the number of cell surface protrusions was increased (Figure S5a,b). Flow cytometry analysis showed a significant increase in both forward scatter (FCS, representing the cell size) and side scatter (SSC, representing the granularity of cells) after L-EC-EV treatment (Figure S5c,d). These phenomena indicated that monocytes undergo changes after L-EC-EV treatment. Next, we found that the F4/80 (a macrophage marker) expression of monocytes detected by western blot and flow cytometry analysis was significantly increased after incubation with L-EC-EVs (Figure 4a,b), indicating the differentiation of monocytes into macrophages. The expression of M1 markers (CD80 and CD86) and M2 markers (CD206 and CD163) of F4/80⁺ cells was detected by flow cytometry. The data indicated a significant increase in the M1 marker expression (Figure 4c), a

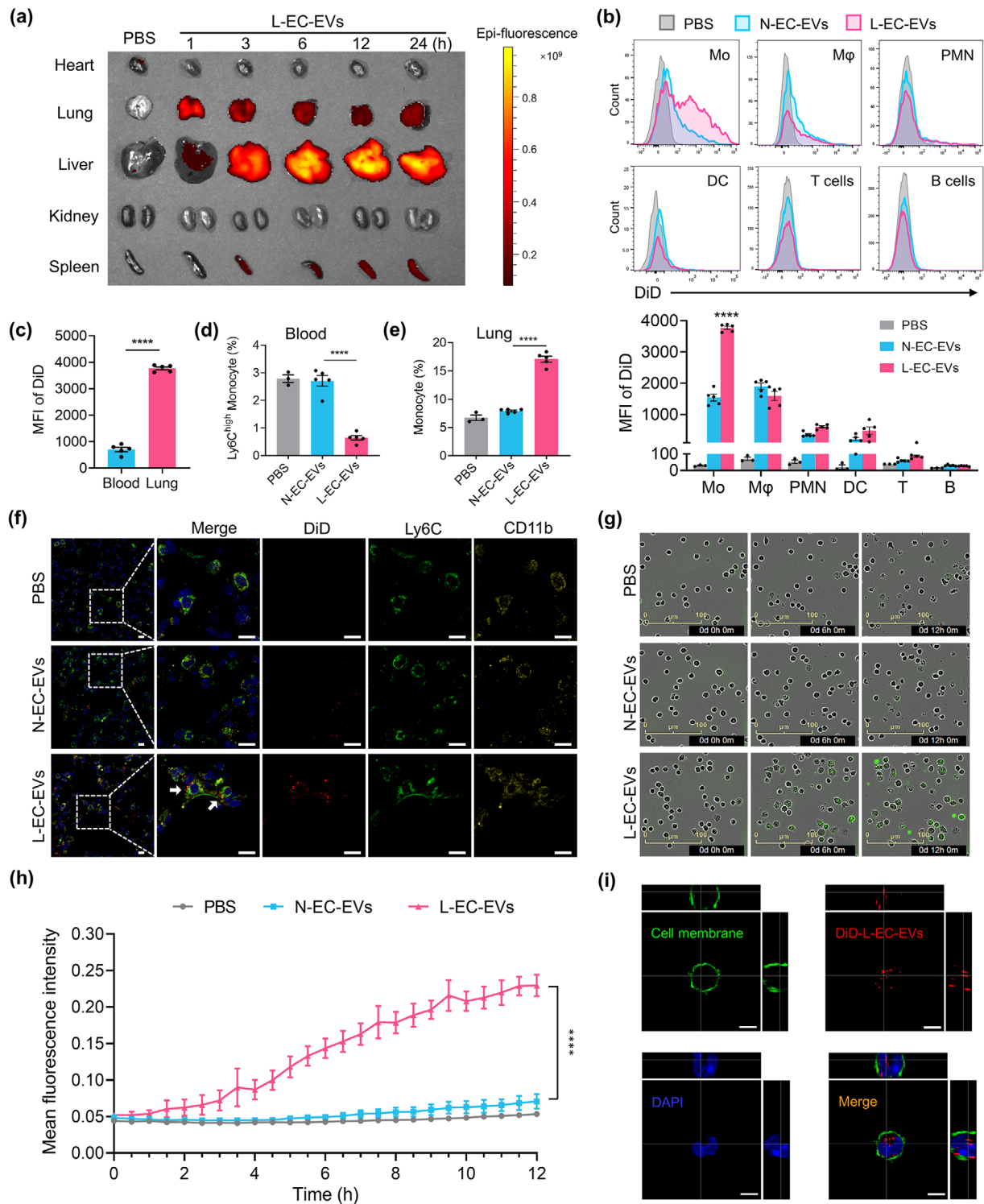


FIGURE 2 The preferential uptake of L-EC-EVs by monocytes. (a) Representative fluorescence image showing the distribution of DiD-labelled L-EC-EVs in different organs at different time points after injection. (b) Distribution of DiD-labelled EC-EVs in various immune cells at 1 h after injection, and quantitative analysis of the amount of DiD-EC-EVs taken up by cells in the lung. (c) Quantitative analysis of the amount of DiD-EC-EVs taken up by monocytes in the blood and lung. (d) The percentage of Ly6C^{high} monocytes in blood. (e) The percentage of monocytes in leukocytes outside neutrophils in the lung. (f) Representative confocal images showing the distribution of DiD-labelled EVs in the lung. Red fluorescent spots indicate DiD-labelled EVs. Monocytes were immunostained with antibodies against Ly6C (green) and CD11b (yellow). Scale bar: 15 μm . (g) Representative images of EC-EVs taken up by monocytes at different time points. The green fluorescent spots indicate PKH67-labelled EVs. (h) Quantitative analysis of the amount of EC-EVs taken up by monocytes over time. (i) Representative images showing the uptake of DiD-labelled EVs by monocytes through confocal laser microscopy assay and z-axis scanning. Scale bar: 5 μm , **** $p < 0.0001$.

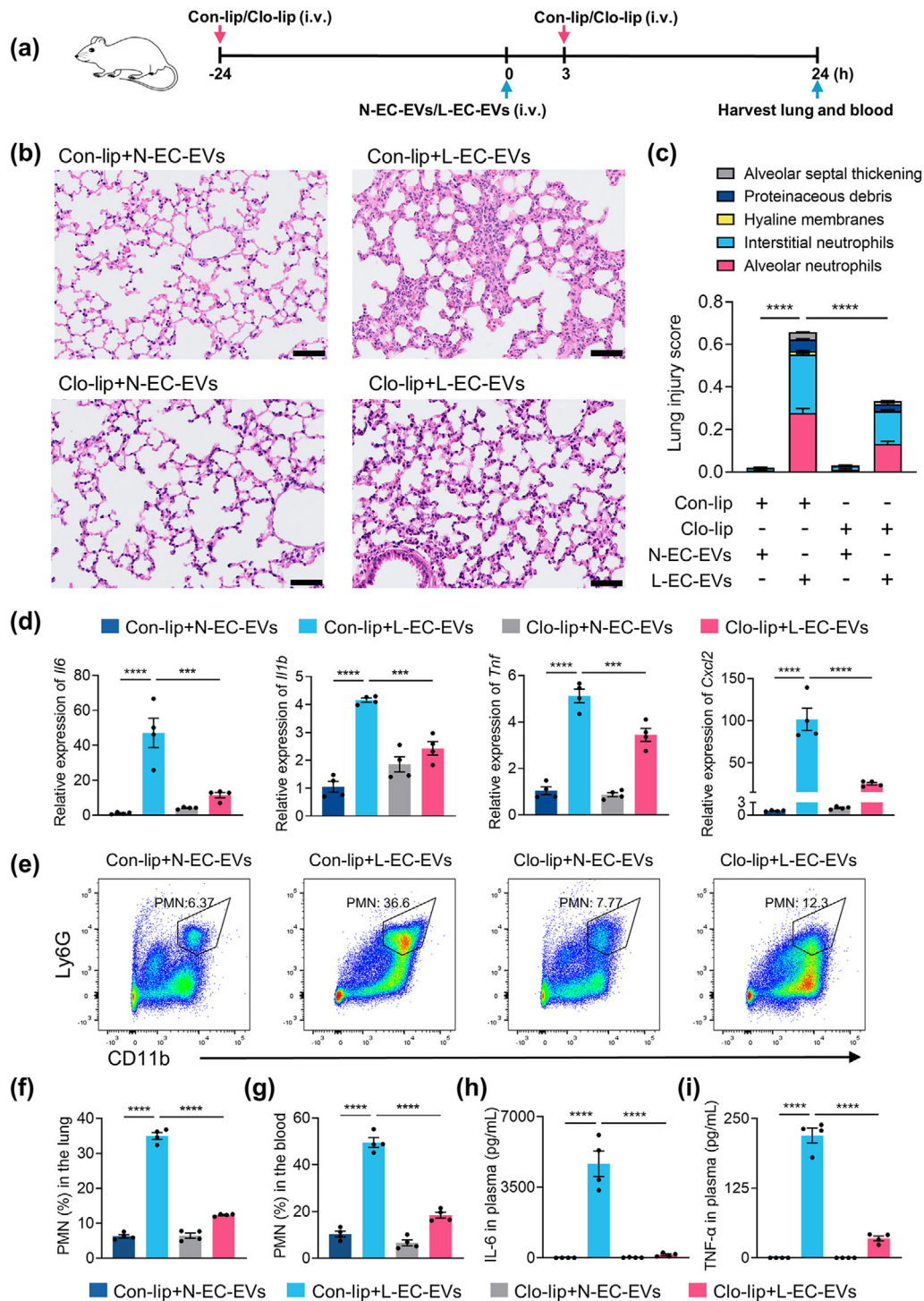


FIGURE 3 The importance of monocytes in the development of ALI caused by L-EC-EVs. (a) Schematic diagram of the experimental design. Briefly, mice were injected with clodronate liposomes (Clo-lip) or control liposomes (Con-lip) via the tail vein 24 h before and 3 h after EV treatment to deplete monocytes, and mice were euthanized at 24 h after EV treatment to assess the extent of lung injury and inflammation. (b) Representative H&E histological images of lung tissues. Scale bar: 50 μ m. (c) The total lung injury score of lung sections from each group. (d) The mRNA levels of inflammatory cytokines and chemokines in lung tissues measured by qRT-PCR. (e) Representative flow cytometry plots of neutrophils in lung tissues. (f, g) Statistical analysis of the proportion of neutrophils among leukocytes (CD45⁺ cells) in lung tissues (f) and blood (g). (h, i) Cytokine levels of IL-6 (h) and TNF- α (i) in plasma were quantified by ELISA. *** p < 0.001, **** p < 0.0001.

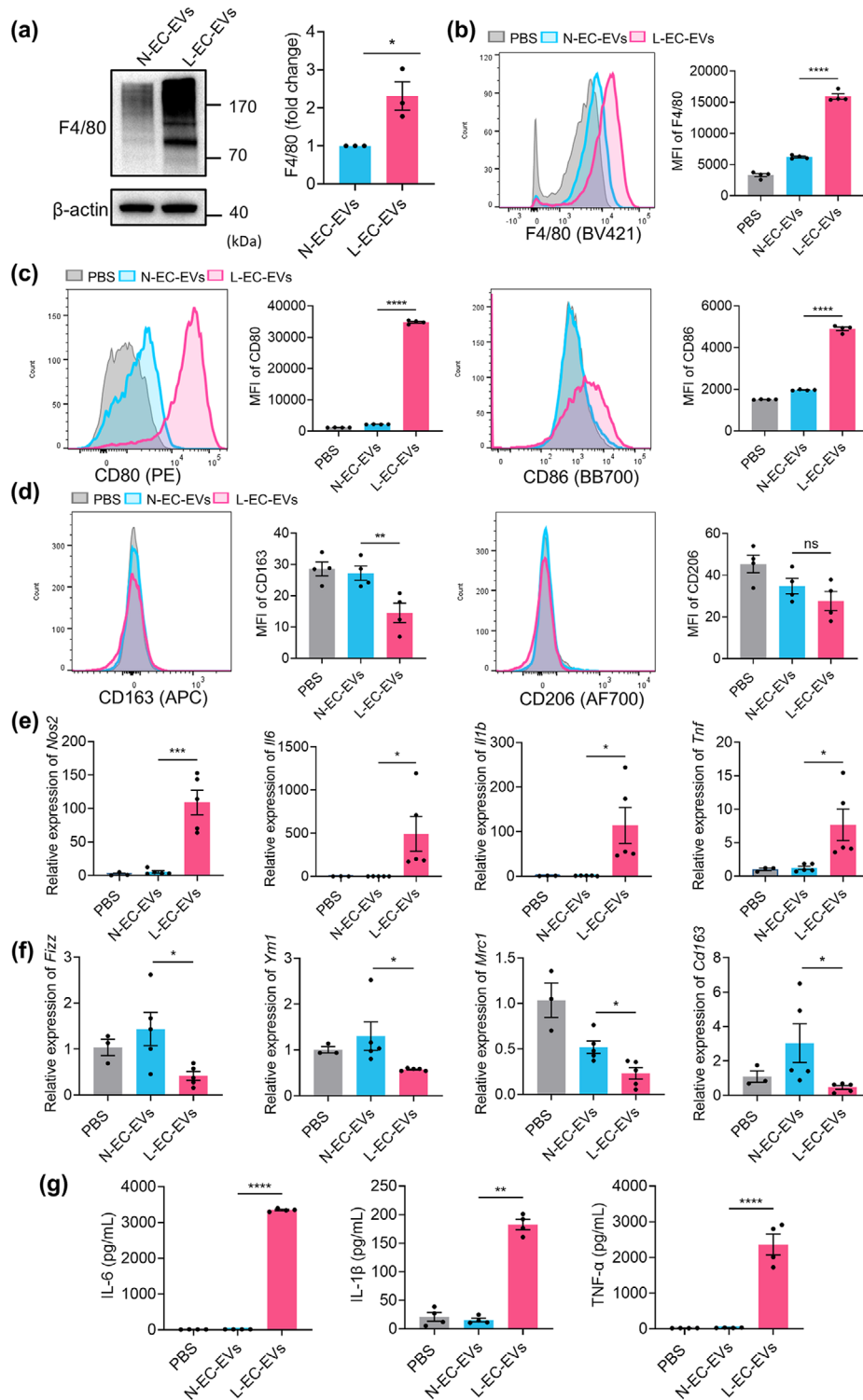


FIGURE 4 Effects of EC-EVs on the differentiation of monocytes. (a) Western blot assay to measure the expression of F4/80 (macrophage marker) in monocytes incubated with N-EC-EVs or L-EC-EVs. (b) Flow cytometry analysis of F4/80 on monocytes. (c) Flow cytometry analysis of M1 markers (CD80 and CD86) on monocyte derived macrophages. (d) Flow cytometry analysis of M2 markers (CD163 and CD206) on monocyte derived macrophages. (e) The mRNA levels of the M1 markers *Nos2*, *Il6*, *Il1b* and *Tnf* were analysed by qRT-PCR. (f) The mRNA levels of the M2 markers *Fizz*, *Ym1*, *Mrc1* and *Cd163* were measured by qRT-PCR. (g) Cytokine levels of IL-6, IL-1 β and TNF- α in the monocyte culture supernatants were quantified by ELISA 24 h after coincubation with EC-EVs. ns: not significant, * $p < 0.05$, ** $p < 0.01$, *** $p < 0.001$, **** $p < 0.0001$.

significant decrease in CD163 expression, and a trend of decreasing CD206 expression upon L-EC-EV treatment (Figure 4d). At the gene expression level, we observed significantly increased expression of M1 markers (*Nos2*, *Il6*, *Il1b*, and *Tnf*) (Figure 4e) and significantly decreased expression of M2 markers (*Fizz*, *Ym1*, *Mrc1*, and *Cd163*) upon L-EC-EV treatment (Figure 4f). In addition, the levels of proinflammatory cytokines, predominantly secreted by M1 macrophages, were significantly increased (Figure 4g). We also used human endothelial cells and monocytes to repeat the phenotyping experiment, and the results were similar to the above outcomes (Figure S6). Altogether, these results provide strong evidence that L-EC-EVs can drive the differentiation of monocytes towards M1 macrophages in vitro.

3.5 | L-EC-EVs promote the differentiation of monocytes into M1-type macrophages in the lung

The effects of EC-EVs on monocytes were also examined in vivo. Mice were intravenously injected with PBS, N-EC-EVs or L-EC-EVs, and lung tissues were collected 24 h later. Immunofluorescence staining of lung tissue sections showed an increase in the number of iNOS⁺ macrophages (M1 type) and a decrease in the number of CD206⁺ macrophages (M2 type) after L-EC-EV treatment (Figure 5a). The phenotypes of the Mo-Mφs and TR-Mφs in lung tissues were further analysed by flow cytometry using specific markers (Figure 5b). The data showed a significant increase in the percentage of macrophages, especially Mo-Mφs, after L-EC-EV injection (Figure 5c,d), with greatly increased expression of CD80 and decreased expression of CD163 on Mo-Mφs, while there was no significant change on TR-Mφs (Figure 5e-h). These results indicate that L-EC-EVs promote the differentiation of Mo-Mφs into M1 phenotype in the lung.

3.6 | L-EC-EVs reprogram monocytes via the classical NF-κB signalling pathway

To further explore the mechanism by which L-EC-EVs regulate monocyte differentiation, N-EC-EV and L-EC-EV treated monocytes were subjected to RNA sequencing. As shown in Figure 6a, a total of 2897 differentially expressed genes were identified. The heatmap revealed upregulation of numerous genes encoding chemokines and proinflammatory cytokines (Figure 6b). KEGG pathway analysis indicated that the NF-κB signalling pathway ranked first among pathways enriched based on the differentially expressed genes that were upregulated (Figure 6c). *Nfκb1* and *Rela* were identified by the Metascape platform as the two transcription factors that were most closely related to the differentially expressed genes that were upregulated (Figure 6d), both of them are transcription factors involved in the NF-κB signalling pathway (Yu et al., 2020). Gene set enrichment analysis (GSEA) also demonstrated that the NF-κB signalling pathway was significantly upregulated when monocytes were incubated with L-EC-EVs (Figure 6e). Next, we used immunofluorescence staining and confirmed that L-EC-EVs promoted the nuclear translocation of p65 in monocytes (Figure 6f). Western blot analysis showed that L-EC-EVs induced the phosphorylation of p65 and IκBα, as well as the degradation of IκBα in monocytes (Figure 6g), indicating activation of the NF-κB pathway. In addition, a multiplexed Luminex assay was used to evaluate the levels of cytokines secreted by monocytes incubated with EC-EVs in the presence or absence of Bay11-7082 (an NF-κB inhibitor) pretreatment, and the results showed that blocking NF-κB activation decreased the secretion of most proinflammatory cytokines and chemokines induced by L-EC-EVs (Figure 6h). Collectively, these results indicate that L-EC-EVs reprogram monocytes via the classical NF-κB signalling pathway.

3.7 | L-EC-EVs facilitate monocyte-mediated proinflammation through VCAM1

In order to clarify the key molecules that function on L-EC-EVs, we subjected N-EC-EVs and L-EC-EVs to proteomic analysis. A total of 67 upregulated proteins and 22 downregulated proteins were screened (Figure 7a). The Venn diagram shows the common KEGG pathways (Table S2) enriched by upregulated EV proteins and the top 100 upregulated monocyte genes (Figure 7b). The NF-κB pathway was the only signal transduction pathway identified, and VCAM1 was the differentially expressed protein with the highest fold change among upregulated proteins. We confirmed by western blot and ELISA that VCAM1 was significantly highly expressed on L-EC-EVs (Figure 7c,d).

To further confirm whether VCAM1 on L-EC-EVs regulates monocyte differentiation, we established a stable VCAM1-knockdown endothelial cell line to produce L-EC-EVs with low expression of VCAM1 (VCAM1-KD L-EC-EVs) and a negative control endothelial cell line to obtain L-EC-EVs with normal VCAM1 expression (NC L-EC-EVs). We first verified that the cell line was successfully established (Figure S7) and that the content of VCAM1 on VCAM1-KD L-EC-EVs was significantly lower than that on NC L-EC-EVs (Figure 7e), then monocytes were incubated with these two EVs respectively. We found that NC L-EC-EVs could enhance the phosphorylation of p65 and IκBα and the secretion of inflammatory factors, while VCAM1-KD L-EC-EVs reversed the increase (Figure 7f), confirming that VCAM1 on L-EC-EVs could activate the NF-κB pathway. Furthermore, mice were injected intravenously with PBS/NC L-EC-EVs/VCAM1-KD L-EC-EVs, and analyses were performed 24 h later. Lung histopathology results showed that VCAM1-KD L-EC-EVs reduced the severity of lung injury and inflammation

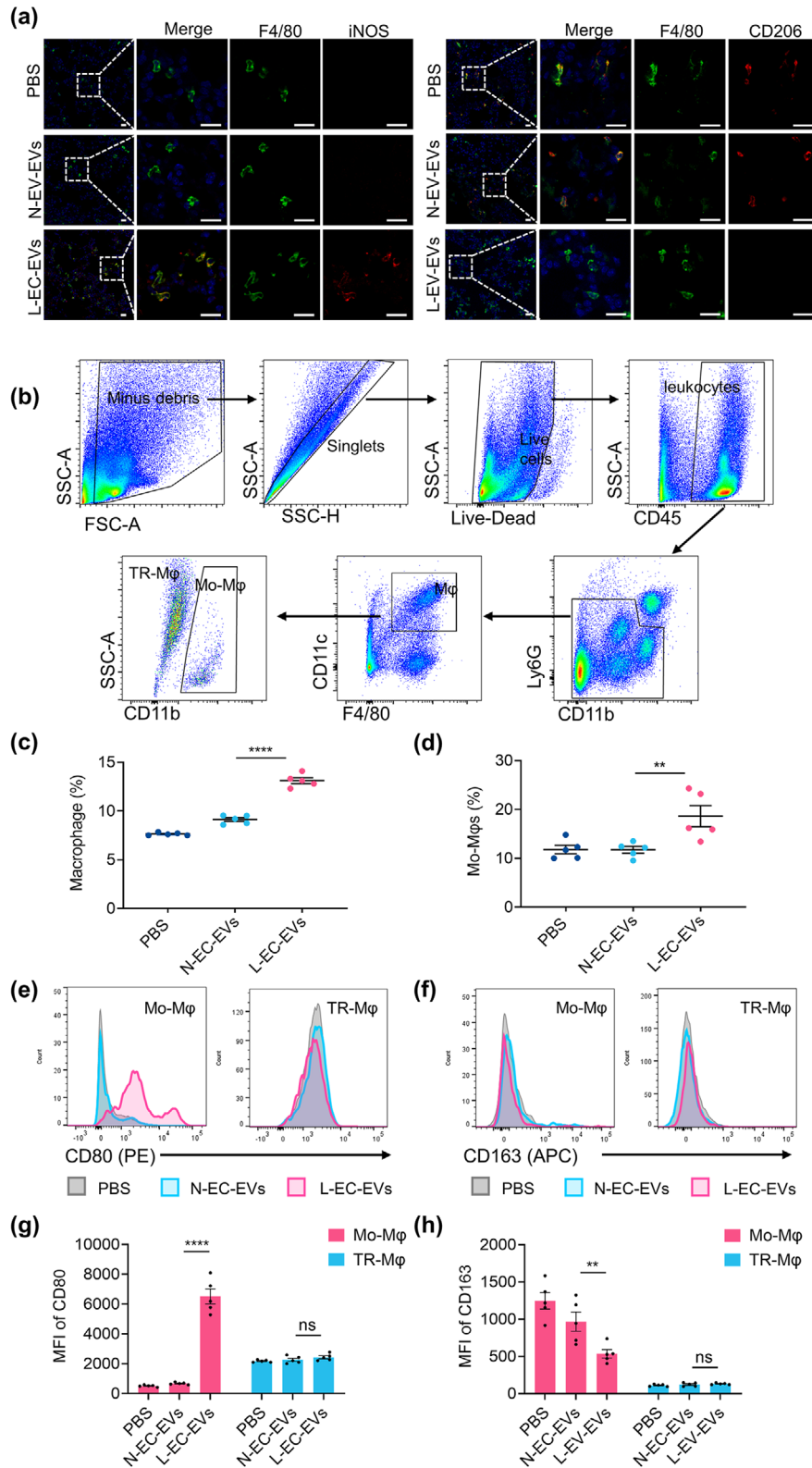


FIGURE 5 The effects of EC-EVs on pulmonary macrophage polarization. (a) Representative immunofluorescence images of lung tissues costained with DAPI, F4/80 (green) and the M1 marker iNOS (red) or M2 marker CD206 (red). (b) Gating strategy of the flow cytometry analysis to identify monocyte-derived macrophages (Mo-Mφs, $CD45^+Ly6G^-F4/80^+CD11c^+CD11b^{high}$) and tissue resident macrophages (TR-Mφs, $CD45^+Ly6G^-F4/80^+CD11c^+CD11b^{low}$). (c) The percentage of macrophages in leukocytes outside neutrophils. (d) The percentage of Mo-Mφs in macrophages. (e, f) Flow cytometric histogram showing the expression of CD80 (M1 marker) and CD163 (M2 marker) on Mo-Mφs and TR-Mφs. (g, h) Quantification of the MFI of CD80 and CD163 expression on Mo-Mφs and TR-Mφs. ns: not significant, ** $p < 0.01$, **** $p < 0.0001$.

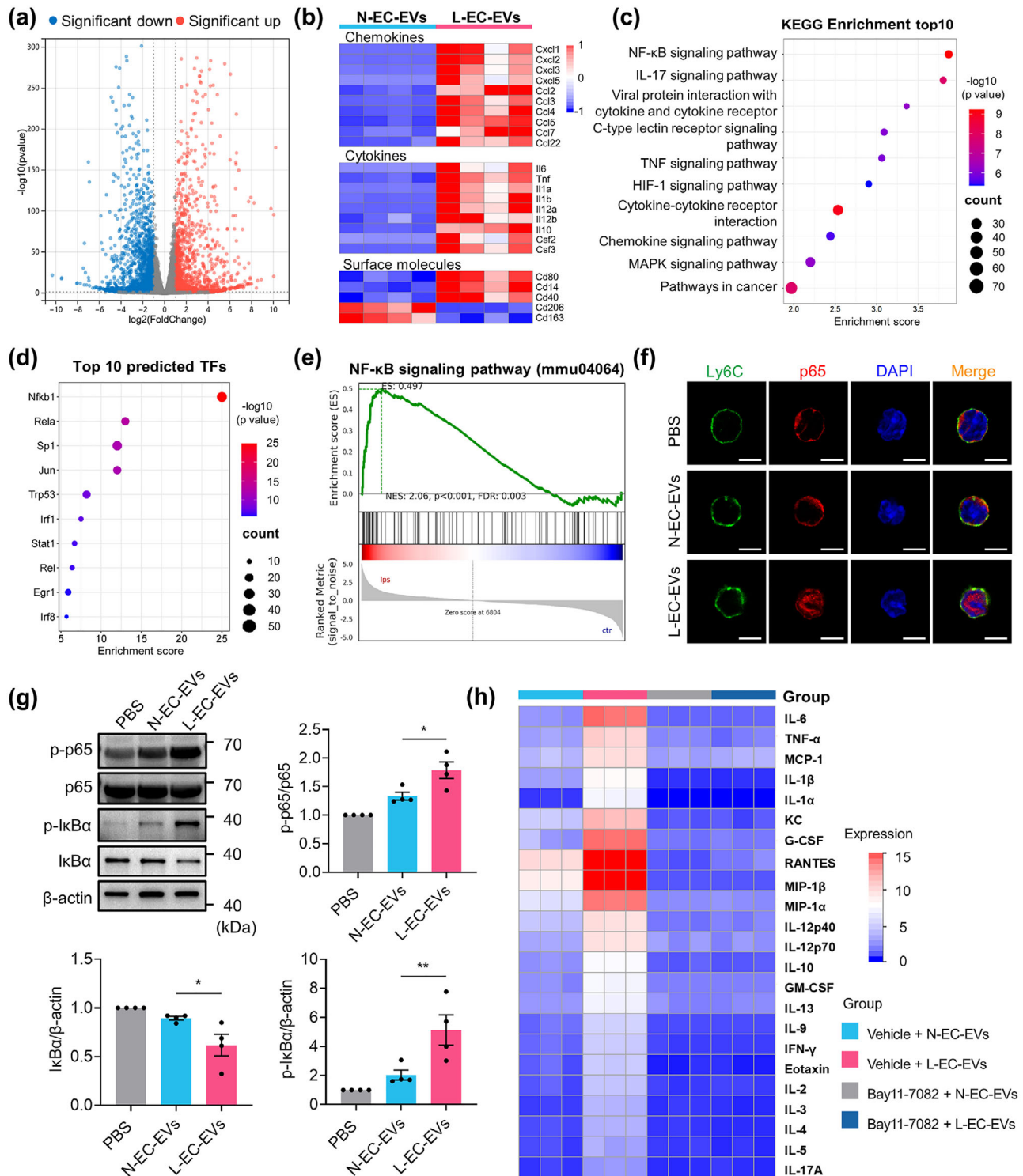


FIGURE 6 L-EC-EVs reprogram monocytes through the NF- κ B pathway. (a) Volcano plot displaying differentially expressed genes between monocytes incubated with N-EC-EVs or L-EC-EVs. Statistical significance was defined as a p value < 0.05 and $|\log_2FC| > 1$. (b) Heatmap showing the expression of genes including cytokines, chemokines and surface molecules. (c) The top 10 KEGG pathways enriched by upregulated differentially expressed genes. (d) Bubble plot showing the top 10 predicted transcription factors of upregulated differentially expressed genes. The size and colour of the dots indicate gene number and p value. (e) GSEA of enrichment for signatures associated with the NF- κ B signalling pathway. (f) Confocal microscopy of p65 localization in monocytes. Scale bar: 5 μ m. (g) Western blot analysis validating p65 phosphorylation (p-p65), I κ B α phosphorylation (p-I κ B α) and I κ B α degradation in monocytes following treatment with EC-EVs for 3 h. (h) Heatmap showing cytokine profiles of monocytes incubated with EC-EVs in the presence or absence of Bay11-7082 (NF- κ B inhibitor) pretreatment. * $p < 0.05$, ** $p < 0.01$.

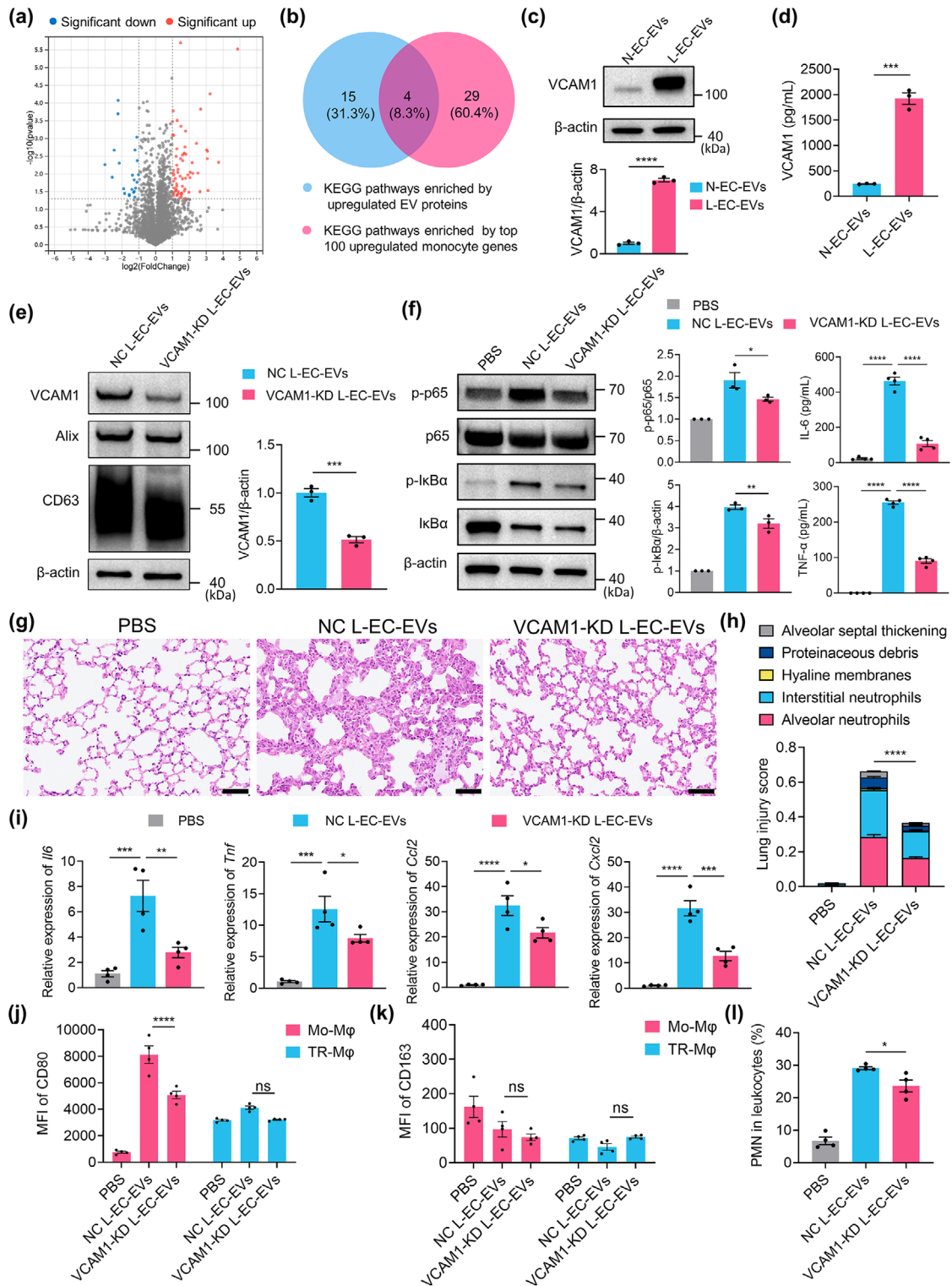


FIGURE 7 VCAM1 on L-EC-EVs contributes to monocyte differentiation and ALI. (a) Volcano plot showing differentially expressed proteins between N-EC-EVs and L-EC-EVs. Statistical significance was defined as a p value < 0.05 and $|\log_2FC| > 1$. (b) Venn diagram showing the KEGG pathways enriched by upregulated EV proteins and the top 100 upregulated monocyte genes. (c) Western blot analysis of VCAM1 in EC-EVs. (d) The level of VCAM1 on EC-EVs (10¹¹ particles/mL) quantified by ELISA. (e) Western blot analysis validating the expression of VCAM1 in EVs. (f) Western blot assay to measure the phosphorylation of p65 (p-p65) and $I\kappa B\alpha$ (p-I $\kappa B\alpha$) in monocytes incubated with different L-EC-EVs, and the secreted levels of inflammatory factors (IL-6 and TNF- α) were measured by ELISA. (g) Representative histological images of lung sections with H&E staining. Scale bar: 50 μ m. (h) The total lung injury score of lung sections from each group. (i) The mRNA levels of *Il6*, *Tnf*, *Ccl2* and *Cxcl2* measured by qRT-PCR. (j, k) Quantification of the expression of CD80 (M1 marker) and CD163 (M2 marker) on Mo-M ϕ s and TR-M ϕ s in lung tissues by flow cytometry. (l) Flow cytometry analysis of neutrophils in lung tissues. ns: not significant, * $p < 0.05$, ** $p < 0.01$, *** $p < 0.001$, **** $p < 0.0001$.

compared to NC L-EC-EVs (Figure 7g, h). Moreover, the mRNA levels of inflammatory cytokines (*Il6* and *Tnf*) and chemokines (*Ccl2* and *Cxcl2*) in the lung tissues were also significantly lower in the VCAM1-KD L-EC-EV-treated group than that in the NC L-EC-EV-treated group (Figure 7i). In addition, flow cytometric analysis showed decreased expression of CD80 on Mo-M ϕ s, no significant change on TR-M ϕ s, and a decreased proportion of neutrophils in the lung tissues of the VCAM1-KD L-EC-EV-treated group compared with the NC L-EC-EV-treated group (Figure 7j–l). Blocking VCAM1 could also attenuated the differentiation of monocytes into M1 macrophages induced by L-EC-EVs (Figure S8). These results suggest that VCAM1-bearing L-EC-EVs facilitate the differentiation of Mo-M ϕ s to the M1 type in the lung via the NF- κ B signalling pathway, which in turn leads to ALI.

3.8 | VCAM1 on L-EC-EVs reprograms monocytes by acting on ITGA4

In the aforementioned results, we made an intriguing observation that injection of L-EC-EVs via the tail vein had no effect on the phenotype of TR-M ϕ s in the lung (Figure 5e–h). To further investigate the role of TR-M ϕ s in ALI caused by L-EC-EVs, Clo-lip or Con-lip were intratracheally injected 24 h before EV treatment (Figure S9a). The effective depletion of TR-M ϕ s in lung tissues was confirmed by flow cytometry analysis (Figure S9b). The pathogenicity of L-EC-EVs persisted after the injection of Con-lip (Figure S9c–i). Of note, the mRNA level of *Cxcl2* in lung tissues, induced by L-EC-EVs, further increased after TR-M ϕ depletion (Figure S9g). These results confirmed that TR-M ϕ s did not mediate the development of ALI caused by L-EC-EVs; in fact, they exerted some protective effects, which was quite different from the effects of monocytes.

To eliminate the effect of the mode of administration or other in vivo factors on the results, equal numbers of monocytes and pulmonary TR-M ϕ s were isolated from WT mice and cocultured with equal amounts of EC-EVs for 24 h. The purity of isolated TR-M ϕ s exceeded 95% (Figure S10a). Light microscopic observation and flow cytometry results displayed no significant changes in the morphology and size of TR-M ϕ s treated with L-EC-EVs (Figure S10b–e), which differed from the monocyte results (Figure S5). Flow cytometry analysis showed a significantly increase in the expression of M1 markers (CD80 and CD86) on L-EC-EV-treated monocytes, while there was no significant change of M1 marker expression on TR-M ϕ s, which was consistent with our in vivo results (Figure 8a).

Using the online Lung Endothelial Cell Atlas data mining website (<http://www.LungEndothelialCellAtlas.com>, Schupp et al., 2021), we found that ITGA4 (a receptor for VCAM1) expression was much higher on monocytes than TR-M ϕ s in healthy human lung tissues (Figure 8b). Flow cytometry analysis confirmed that the expression of ITGA4 on the monocyte surface was significantly higher than that of TR-M ϕ s (Figure 8c). Immunofluorescence staining also indicated abundant distribution of ITGA4 on the surface of monocytes (showing a fluorescent ring pattern), while only a few scattered fluorescent spots were observed on TR-M ϕ s (Figure 8d). In addition, flow cytometry analysis confirmed that the fluorescence signal of ITGA4 was highly expressed on the surface of Mo-M ϕ s in the lungs of septic mice, but almost undetectable on TR-M ϕ s (Figure S11). Next, we pretreat monocytes with an anti-ITGA4 blocking antibody before incubation with L-EC-EVs. The results showed that the phosphorylation of p65 in monocytes incubated with L-EC-EVs was inhibited upon anti-ITGA4 antibody treatment (Figure 8e), leading to reduced expression of M1 markers (CD80 and CD86) (Figure 8f) and decreased release of inflammatory cytokines (IL-6 and TNF- α) (Figure 8g), indicating that ITGA4 is also involved in the activation of the NF- κ B signalling pathway. Flow cytometry analysis also revealed that administration of an anti-ITGA4 antibody reversed the increase in the expression of M1 markers (CD80 and CD86) and the decrease in the expression of a M2 marker (CD206) on pulmonary Mo-M ϕ s of L-EC-EV-treated mice (Figure 8h). These results strongly indicate that VCAM1 on L-EC-EVs reprograms monocytes rather than TR-M ϕ s by targeting ITGA4 on the surface of monocytes.

In addition, to explore the role of endogenous EC-EVs, we added groups of mice that only underwent CLP or sham-operation without EV injection. As shown in Figure S12a, the levels of VCAM1⁺ EC-EVs were significantly increased in CLP-induced septic mice compared with the sham-operated mice. Flow cytometry analysis revealed that blocking VCAM1 or ITGA4 could reverse the increase of the expression of the M1 marker (CD80) and the decrease of expression of the M2 marker (CD163) on Mo-M ϕ s in lung tissues of septic mice (Figure S12b, c). These results indicate that the VCAM-1 and ITGA4 signalling pathway may be activated by endogenous EC-EVs in sepsis.

3.9 | Numbers of circulating endothelial cell-derived VCAM1⁺ EVs are increased in patients with sepsis-related ARDS

Based on the above findings, we returned to the clinic to validate quantitative changes in VCAM1⁺ EC-EVs in human samples. We isolated plasma EVs from patients with ARDS due to non-pulmonary sepsis, patients without ARDS or sepsis (as the patient control group), and healthy volunteers (as normal control group). The main clinical characteristics are shown in Table S3. Western blot analysis confirmed that the expression of VCAM1 in plasma EVs was greatly increased in sepsis-related ARDS patients compared to control patients (Figure 9a). The proportion of VCAM1⁺ EC-EVs in plasma EVs was determined by detecting the expression of both VCAM1 and CD31 using nanoflow cytometry (Figure 9b). The data revealed that the percentage of EC-EVs,

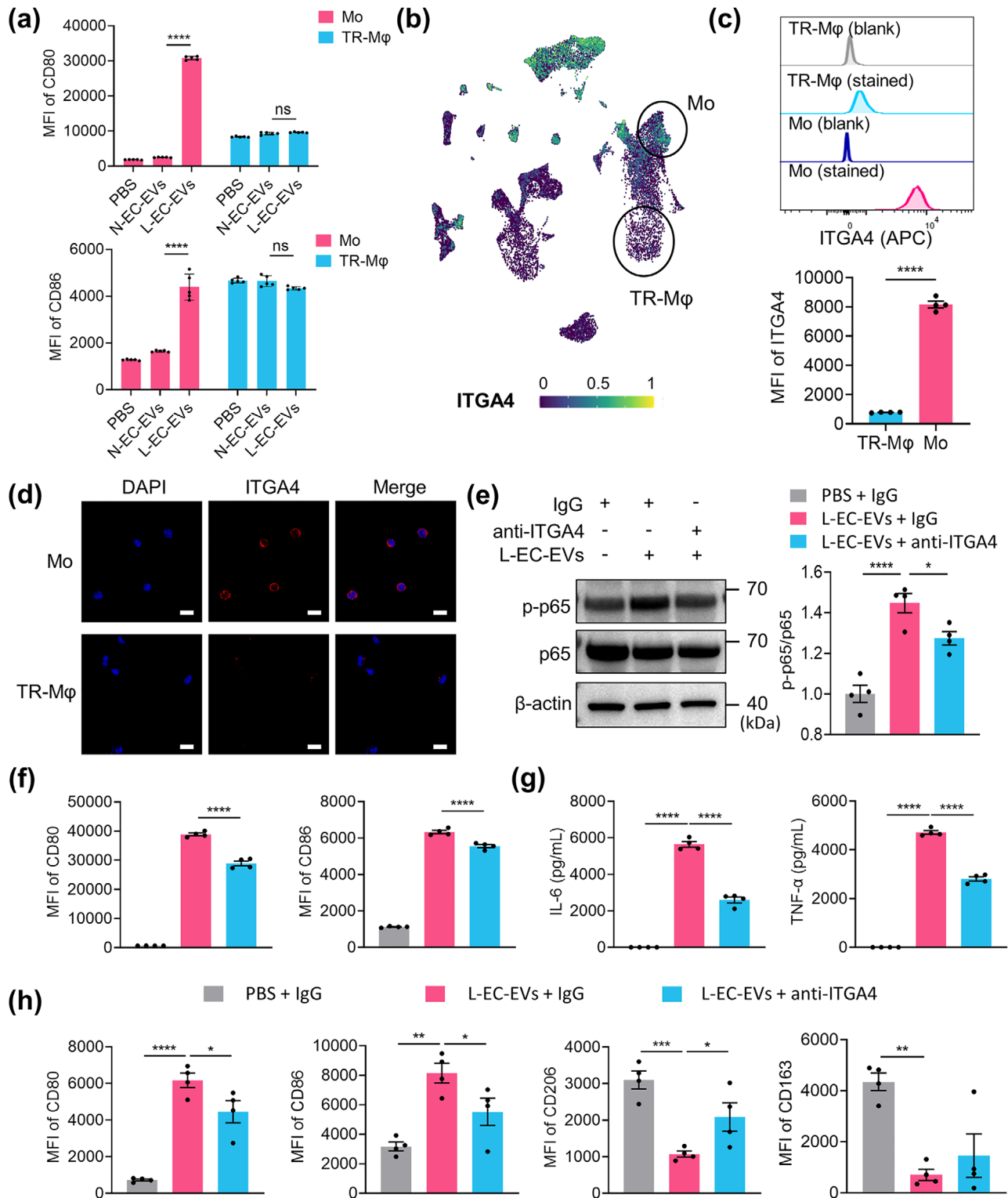


FIGURE 8 VCAM1 on L-EC-EVs regulates monocyte but not TR-M ϕ differentiation by acting on ITGA4. (a) The expression of M1 markers (CD80 and CD86) on monocytes and TR-M ϕ s detected by flow cytometry. (b) UMAP plot of single-cell RNAseq datasets of healthy human lungs showing the expression of ITGA4 in different cell types. The analysis was conducted using the Lung Endothelial Cell Atlas data mining website (<http://www.LungEndothelialCellAtlas.com>). (c) Quantification of the expression of ITGA4 on monocytes and TR-M ϕ s by flow cytometry. (d) Immunofluorescence images showing the expression of ITGA4 (red) on monocytes and TR-M ϕ s cells. Scale bar: 10 μ m. (e–g) Monocytes were pretreated with anti-ITGA4 blocking antibody or IgG isotype control for 1 h, and then incubated with PBS/L-EC-EVs for 24 h. The phosphorylation of p65 (p-p65) in monocytes was detected by western blotting (e), the expression of M1 markers (CD80 and CD86) on cells was measured by flow cytometry (f), and the levels of inflammatory cytokines (IL-6 and TNF- α) were quantified by ELISA (g). (h) Mice were pretreated with either anti-ITGA4 antibody or IgG isotype 4 h before EV treatment. The expression of M1 markers and M2 markers on Mo-M ϕ s in lung tissues was detected by flow cytometry. ns: not significant, * p < 0.05, ** p < 0.01, *** p < 0.001, **** p < 0.0001.

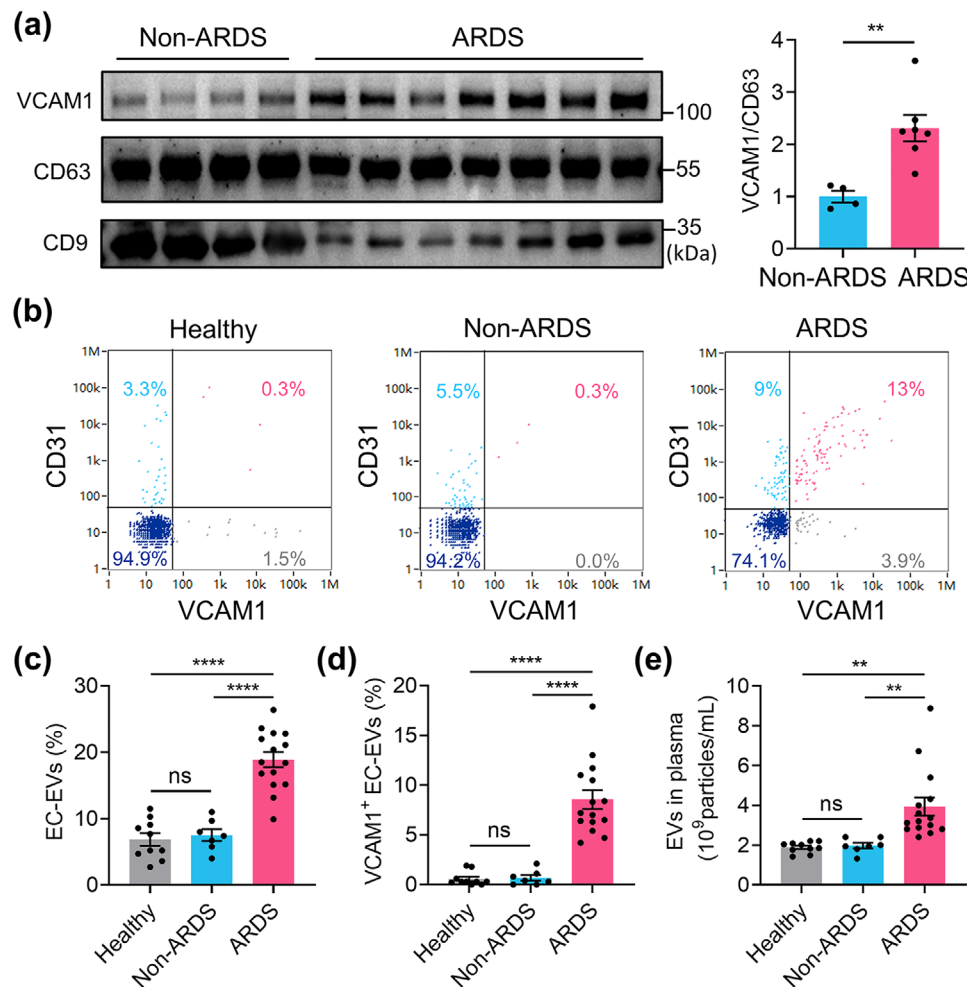


FIGURE 9 Endothelial cell-derived VCAM1⁺ EVs are increased in the plasma of patients with sepsis-related ARDS. (a) Western blot analysis of VCAM1 expression in plasma EVs. (b) Representative dot plot, detected by nanoflow cytometry, showing the percentage of VCAM1⁺ EC-EVs in plasma EVs of healthy volunteers, non-ARDS patient and sepsis-related ARDS patients. (c, d) Quantification of the percentage of EC-EVs (c) and VCAM1⁺ EC-EVs (d) in plasma EVs. (e) Quantification of EVs isolated from the plasma of sepsis-related ARDS patients and controls. ns: not significant, ** $p < 0.01$, **** $p < 0.0001$.

especially VCAM1⁺ EC-EVs, in the plasma of patients with sepsis-related ARDS was much higher than that in the plasma of controls (Figure 9c, d). Moreover, the concentration of plasma EVs was higher in patients with sepsis-related ARDS than that in the two control groups (Figure 9e). These results demonstrate at the clinical level that circulating VCAM1⁺ EC-EVs are increased in patients with sepsis-related ARDS.

4 | DISCUSSION

ALI/ARDS is a critical global medical challenge, commonly seen in ICU, and is characterized by excessive and overwhelming uncontrolled inflammatory reactions within the lung. Sepsis-related ARDS is the main type of ARDS with a higher mortality rate than other types. However, there is still no clinically effective pharmacological treatment. In this study, we identified a significant increase in the number of circulating EC-EVs during extra-pulmonary sepsis. Notably, these EC-EVs were preferentially taken up by monocytes and reprogrammed into proinflammatory macrophages in the lung, resulting in cytokine storms and infiltration of more inflammatory cells to exacerbate lung injury. However, these EVs had no effect on pulmonary TR-M ϕ s. Bioinformatics analysis and further mechanistic studies suggested that VCAM1, overexpressed on EC-EVs during sepsis, activated the NF- κ B pathway by interacting with ITGA4 on the surface of monocytes but not TR-M ϕ s, thereby reprogramming monocytes (Figure 10). Moreover, at the clinical level, we confirmed a significant increase in VCAM1⁺ EC-EV numbers in patients with sepsis-related ARDS, which could serve as a potential biomarker and target for the development of ARDS in septic patients.

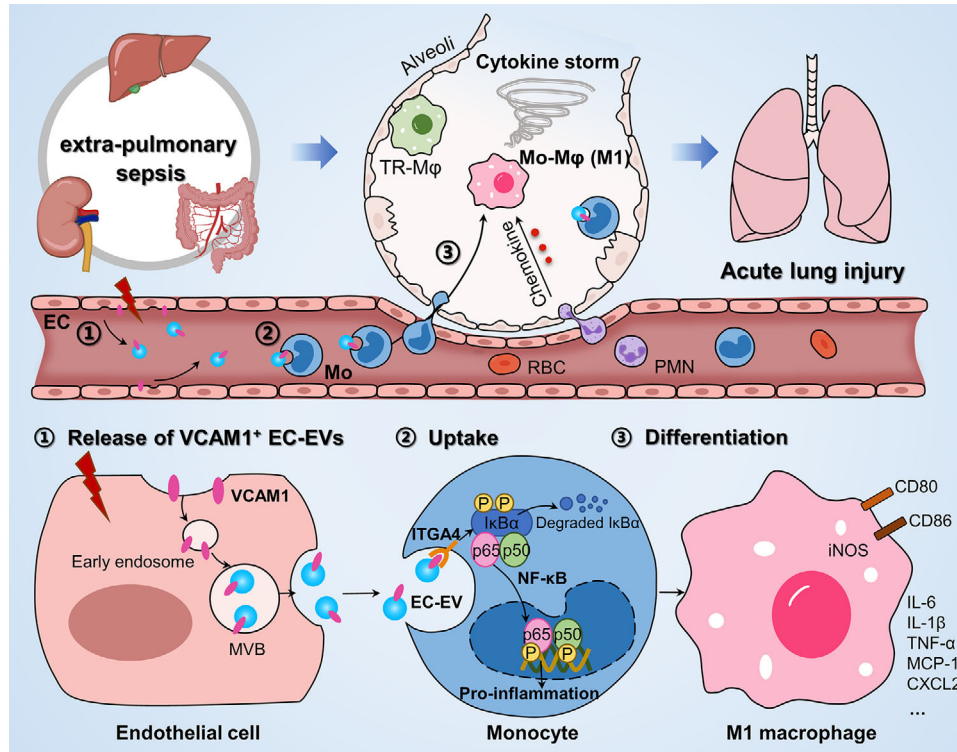


FIGURE 10 Schematic illustration of the effects of EC-EVs in sepsis-related ALI/ARDS. In extra-pulmonary sepsis, the number of VCAM1⁺ EVs released by endothelial cells was increased, and they were preferentially taken up by monocytes in the lung. VCAM1, highly expressed on these EVs, activates the NF- κ B pathway by acting on ITGA4, thus promoting the differentiation of monocytes into M1-type macrophages. The latter secreted much proinflammatory cytokines and chemokines, recruiting more inflammatory cells to amplify the inflammatory response and further exacerbate ALI. EC: endothelial cell; Mo: monocyte; PMN: polymorphonuclear neutrophil; RBC: red blood cell; Mo-M ϕ : monocyte-derived macrophage; TR-M ϕ : tissue resident macrophages; MVB: multivesicular body.

4.1 | EC-EVs are crucial mediators to induce sepsis-related ARDS

EVs are increasingly considered an important form of cell-to-cell communication that functions without the need for direct cell contact (Urabe et al., 2021). EVs can exert long-distance effects, and play a critical role in the pathogenesis of inflammatory pulmonary diseases (Hu et al., 2022). It has been reported that EVs originating from different cells preferentially interact with specific cell types, and the selective uptake of EVs is critical for their function (French et al., 2017). In this study, we ascertained that intravenously injected L-EC-EVs were first detected and maintained at relatively high levels in the lung tissue. Notably, L-EC-EVs specifically targeted monocytes among immune cells to induce ALI. These findings reveal the tissue specificity and cell specificity of the actions of L-EC-EVs, providing insights into why lung tissue is the earliest and most susceptible organ to be damaged in sepsis.

Due to technical limitations, most previous studies focused on large EC-EVs (also called microparticles), while the number and function of small EC-EVs (mainly composed of exosomes) under inflammatory stimulation are not fully clear. These two populations have distinct formation mechanisms and particle sizes. Small EVs are more likely to cross the human body barriers than large EVs and have the characteristics such as a wide range of effects, resistance to content degradation, and low immunogenicity (Shao et al., 2018). In this study, we used differential ultracentrifugation to obtain small EC-EVs and conducted an in-depth investigation into their functions. Our research has filled the gap in this field to some extent.

Our study revealed that VCAM1 overexpressed on L-EC-EVs could reprogram the differentiation of monocytes via the NF- κ B signalling pathway. VCAM1 is highly expressed on the surface of endothelial cells in response to inflammatory stimulation, mediating leukocyte-endothelial cell adhesion and playing a crucial role in inflammatory diseases (Furuta et al., 2021). Previous studies demonstrated that VCAM1 mainly functions through direct contact between cells, while our findings introduce a novel mode of action for VCAM1. Additionally, recent studies have reported elevated plasma levels of VCAM1 in patients with severe COVID-19 pneumonia (Blot et al., 2021). In our clinical study, we confirmed a significant increase in EC-EVs, especially VCAM1⁺ EC-EVs, in the plasma of patients with sepsis-related ARDS, suggesting their potential as clinical biomarkers.

In addition to proteins like VCAM1, EVs can regulate the function of target cells by transferring other molecules, such as mRNAs, miRNAs, tRNAs, or other noncoding RNAs (O'Brien et al., 2020; van Niel et al., 2022). Hence, we cannot rule out the

possibility that other molecules within the EC-EVs, such as different RNAs, may also influence the development of sepsis-related ALI/ARDS by affecting monocyte phenotypes. Moreover, EVs are released by various cell types, such as platelets, monocytes, and lymphocytes. How EVs derived from different cells exert their functions during ALI/ARDS needs to be further explored.

Notably, among the numerous cytokines with significantly elevated secretion levels released by monocytes after incubation with L-EC-EVs (Figure 6h), several can influence the proliferation or differentiation of T cells. For example, IL-6 is the most important cytokine to drive Th17 cell differentiation, and IL-12 promotes Th1 differentiation (Saravia et al., 2019; Yamashita et al., 2011). Studies have reported that abnormal ratio of Th17/Treg or Th2/Th1 cells in peripheral blood or lung tissue can facilitate an uncontrolled inflammatory response in ARDS or sepsis (Li et al., 2015; Xue et al., 2019; Yu et al., 2015). Therefore, in addition to affecting the function of monocyte-macrophage system, L-EC-EVs may further aggravate lung injury by promoting the imbalance of T-cell proliferation or differentiation.

4.2 | Mo-M ϕ s are the key drivers in sepsis-related ALI/ARDS

It was traditionally thought that the functional differences of macrophages were mainly influenced by the tissue microenvironment. In response to different microenvironmental stimuli, monocytes or macrophages can differentiate into either the M1 or the M2 phenotype (Chen et al., 2023). However, emerging evidence shows that the origin of macrophages is also an important factor determining their phenotypes and functions (Li et al., 2022). Recent study suggests that Mo-M ϕ s are important contributors to the excessive inflammatory reaction of lung tissue secondary to infection (Evren et al., 2021). In ALI, TR-M ϕ s act as sentinel cells against incoming pathogens in the early stage and facilitate the resolution of inflammation in the later stage. Notably, the recruited Mo-M ϕ s exert stronger proinflammatory effects and cause greater tissue destruction (Mould et al., 2017). However, the mechanisms underlying such distinct functions between these two types of macrophages are not yet clear.

In this study, we confirmed that depletion of monocyte but not TR-M ϕ s could attenuate the ALI caused by L-EC-EVs. Moreover, we observed that ITGA4, a receptor for VCAM1 (Jacamo et al., 2014; Ross et al., 2006), was highly expressed on the surface of monocytes/Mo-M ϕ s but not TR-M ϕ s, which may explain why L-EC-EVs drove the differentiation of Mo-M ϕ s but not TR-M ϕ s into the M1 type. This insight reveals the distinct roles played by Mo-M ϕ s and TR-M ϕ s, demonstrating that Mo-M ϕ s, rather than TR-M ϕ s, are important drivers of sepsis-related ALI/ARDS. This finding implies that a more precise clinical intervention strategy could be achieved through the selective regulation of Mo-M ϕ s by targeting ITGA4.

4.3 | Limitations and significance

We employed the CLP model, which is simple to operate and reflects polymicrobial infection, making it considered the model closest to human sepsis and the gold standard for sepsis research (Cai et al., 2023). However, the model has several limitations, in particular difficulties in controlling the release of caecal content. To address this, we took some measures, such as using the same needles and maintaining the consistency of the ligation position, to ensure the accuracy of the experimental results. Moreover, clinical studies are limited by small sample sizes, although we have increased the number of both sepsis-related ARDS and control patients, and add a third group of healthy subjects. Encouragingly, the clinical observations were consistent with the results of the animal studies, and further validation in more subjects in the future will strengthen our research.

In summary, our study marks a significant breakthrough in understanding the role of EC-EVs in sepsis-related ALI/ARDS and uncovers a previously unknown mechanism by which extra-pulmonary sepsis could lead to ALI/ARDS. Our findings strongly suggest that eliminating EC-EVs, inhibiting their uptake by monocytes, or blocking VCAM1/ITGA4 in the early stage of infection can reverse the detrimental effects of Mo-M ϕ s and curb the progression of pulmonary inflammation. These findings are expected to provide novel targets and strategies for the precise clinical treatment of sepsis-related ALI/ARDS.

AUTHOR CONTRIBUTIONS

Haibo Qiu; Jie Chao; Lu Wang and **Ying Tang** conceived the project and designed the experiments. Lu Wang and **Jiajian Tang** conducted the experiments. Lu Wang; **Xu Liu** and **Shuangfeng Zi** contributed to the collection of EVs. **Songli Li** was responsible for the collection of clinical samples. **Hanbing Chen** assisted the animal studies. Lu Wang and Ying Tang analysed the results and wrote the manuscript. Haibo Qiu and Jie Chao critically revised and commented on the manuscript. **Airan Liu; Wei Huang; Jianfeng Xie** and **Ling Liu** provided technical support and insightful suggestions. All the authors read and approved the final manuscript.

ACKNOWLEDGEMENTS

This work was supported by the Key Program of the National Natural Science Foundation of China (No. 81930058), the Special Funds of the National Natural Science Foundation of China (No. 82341032), the National Key R&D Program of China (2022YFC2504403, 2021YFC2500804), the Jiangsu Provincial Key Medical Discipline (Laboratory) (ZDXKA2016025),

the Jiangsu Provincial Special Program of Medical Science (BE2019749), and the National Natural Science Foundation of China (No. 82072154). In addition, we appreciate Professor Hong Yang at Tianjin Medical University for her insightful discussions and suggestions.

CONFLICT OF INTEREST STATEMENT

The authors declare no conflict of interest.

DATA AVAILABILITY STATEMENT

All data are available in the main text or the supplementary materials. RNA-seq data are available in the National Center for Biotechnology Information Gene Expression Omnibus (GEO) under accession code GSE236215. The proteomic data have been deposited to the ProteomeXchange Consortium via the iProX repository with the dataset identifier PXD043470.

ORCID

Lu Wang  <https://orcid.org/0009-0003-8866-8610>

Ying Tang  <https://orcid.org/0000-0002-9526-9613>

Haibo Qiu  <https://orcid.org/0000-0001-8589-4717>

REFERENCES

- Baasch, S., Giansanti, P., Kolter, J., Riedl, A., Forde, A. J., Runge, S., Zenke, S., Elling, R., Halenius, A., Brabletz, S., Hengel, H., Kuster, B., Brabletz, T., Cicin-Sain, L., Arens, R., Vlachos, A., Rohr, J. C., Stemmler, M. P., Kopf, M., ... Henneke, P. (2021). Cytomegalovirus subverts macrophage identity. *Cell*, *184*, 3774–3973. <http://doi.org/10.1016/j.cell.2021.05.009>
- Blot, M., de Maistre, E., Bourredjem, A., Quenot, J. P., Nguyen, M., Bouhemad, B., Charles, P. E., Binquet, C., & Piroth, L. (2021). Specific features of the coagulopathy signature in severe COVID-19 pneumonia. *Frontiers In Medicine*, *8*, 675191. <http://doi.org/10.3389/fmed.2021.675191>
- Bohnacker, S., Hartung, F., Henkel, F., Quaranta, A., Kolmert, J., Priller, A., Ud-Dean, M., Giglberger, J., Kugler, L. M., Pechtold, L., Yazici, S., Lechner, A., Erber, J., Protzer, U., Lingor, P., Knolle, P., Chaker, A. M., Schmidt-Weber, C. B., Wheelock, C. E., & Esser-von Bieren, J. (2022). Mild COVID-19 imprints a long-term inflammatory eicosanoid- and chemokine memory in monocyte-derived macrophages. *Mucosal Immunology*, *15*, 515–524. <http://doi.org/10.1038/s41385-021-00482-8>
- Cai, L., Rodgers, E., Schoenmann, N., & Raju, R. P. (2023). Advances in rodent experimental models of sepsis. *International Journal of Molecular Sciences*, *24*, 9578. <http://doi.org/10.3390/ijms24119578>
- Chen, S., Saeed, A. F. U. H., Liu, Q., Jiang, Q., Xu, H., Xiao, G. G., Rao, L., & Duo, Y. (2023). Macrophages in immunoregulation and therapeutics. *Signal Transduction and Targeted Therapy*, *8*, 207. <http://doi.org/10.1038/s41392-023-01452-1>
- Cheng, K. T., Xiong, S., Ye, Z., Hong, Z., Di, A., Tsang, K. M., Gao, X., An, S., Mittal, M., Vogel, S. M., Miao, E. A., Rehman, J., & Malik, A. B. (2017). Caspase-11-mediated endothelial pyroptosis underlies endotoxemia-induced lung injury. *The Journal of Clinical Investigation*, *127*, 4124–4135. <http://doi.org/10.1172/JCI94495>
- Dhaliwal, K., Scholefield, E., Ferenbach, D., Gibbons, M., Duffin, R., Dorward, D. A., Morris, A. C., Humphries, D., MacKinnon, A., Wilkinson, T. S., Wallace, W. A. H., van Rooijen, N., Mack, M., Rossi, A. G., Davidson, D. J., Hirani, N., Hughes, J., Haslett, C., & Simpson, A. J. (2012). Monocytes control second-phase neutrophil emigration in established lipopolysaccharide-induced murine lung injury. *American Journal of Respiratory and Critical Care Medicine*, *186*, 514–524. <http://doi.org/10.1164/rccm.201112-2132OC>
- Evren, E., Ringqvist, E., Tripathi, K. P., Sleiers, N., Rives, I. C., Alisjahbana, A., Gao, Y., Sarhan, D., Halle, T., Sorini, C., Lepzien, R., Marquardt, N., Michaëlsson, J., Smed-Sörensen, A., Botling, J., Karlsson, M. C. I., Villablanca, E. J., & Willinger, T. (2021). Distinct developmental pathways from blood monocytes generate human lung macrophage diversity. *Immunity*, *54*, 259–275. <http://doi.org/10.1016/j.immuni.2020.12.003>
- Fan, E., Brodie, D., & Slutsky, A. S. (2018). Acute respiratory distress syndrome: Advances in diagnosis and treatment. *Jama*, *319*, 698–710. <http://doi.org/10.1001/jama.2017.21907>
- French, K. C., Antonyak, M. A., & Cerione, R. A. (2017). Extracellular vesicle docking at the cellular port: Extracellular vesicle binding and uptake. *Seminars in Cell & Developmental Biology*, *67*, 48–55. <http://doi.org/10.1016/j.semcdb.2017.01.002>
- Furuta, K., Guo, Q., Pavelko, K. D., Lee, J. H., Robertson, K. D., Nakao, Y., Melek, J., Shah, V. H., Hirsova, P., & Ibrahim, S. H. (2021). Lipid-induced endothelial vascular cell adhesion molecule 1 promotes nonalcoholic steatohepatitis pathogenesis. *The Journal of Clinical Investigation*, *131*, e143690. <http://doi.org/10.1172/JCI143690>
- Ginhoux, F., & Guilliama, M. (2016). Tissue-resident macrophage ontogeny and homeostasis. *Immunity*, *44*, 439–449. <http://doi.org/10.1016/j.immuni.2016.02.024>
- Gorman, E. A., O’Kane, C. M., & McAuley, D. F. (2022). Acute respiratory distress syndrome in adults: Diagnosis, outcomes, long-term sequelae, and management. *Lancet (London, England)*, *400*, 1157–1170. [http://doi.org/10.1016/S0140-6736\(22\)01439-8](http://doi.org/10.1016/S0140-6736(22)01439-8)
- Grange, C., & Bussolati, B. (2022). Extracellular vesicles in kidney disease. *Nature Reviews. Nephrology*, *18*, 499–513. <http://doi.org/10.1038/s41581-022-00586-9>
- Guo, Q., Furuta, K., Lucien, F., Gutierrez Sanchez, L. H., Hirsova, P., Krishnan, A., Kabashima, A., Pavelko, K. D., Madden, B., Alhuwaish, H., Gao, Y., Revzin, A., & Ibrahim, S. H. (2019). Integrin β -enriched extracellular vesicles mediate monocyte adhesion and promote liver inflammation in murine NASH. *Journal of Hepatology*, *71*, 1193–1205. <http://doi.org/10.1016/j.jhep.2019.07.019>
- Hou, P. P., Luo, L. J., Chen, H. Z., Chen, Q. T., Bian, X. L., Wu, S. F., Zhou, J. X., Zhao, W. X., Liu, J. M., Wang, X. M., Zhang, Z. Y., Yao, L. M., Chen, Q., Zhou, D., & Wu, Q. (2020). Ectosomal PKM2 promotes HCC by inducing macrophage differentiation and remodeling the tumor microenvironment. *Molecular Cell*, *78*, 1192–1206. <http://doi.org/10.1016/j.molcel.2020.05.004>
- Hu, Q., Zhang, S., Yang, Y., Yao, J. Q., Tang, W. F., Lyon, C. J., Hu, T. Y., & Wan, M. H. (2022). Extracellular vesicles in the pathogenesis and treatment of acute lung injury. *Military Medical Research*, *9*, 61. <http://doi.org/10.1186/s40779-022-00417-9>
- Jacamo, R., Chen, Y., Wang, Z., Ma, W., Zhang, M., Spaeth, E. L., Wang, Y., Battula, V. L., Mak, P. Y., Schallmoser, K., Ruvoilo, P., Schober, W. D., Shpall, E. J., Nguyen, M. H., Strunk, D., Bueso-Ramos, C. E., Konoplev, S., Davis, R. E., Konopleva, M., & Andreeff, M. (2014). Reciprocal leukemia-stroma VCAM-1/VLA-4-dependent activation of NF- κ B mediates chemoresistance. *Blood*, *123*, 2691–2702. <http://doi.org/10.1182/blood-2013-06-511527>

- Kim, D., Langmead, B., & Salzberg, S. L. (2015). HISAT: A fast spliced aligner with low memory requirements. *Nature Methods*, *12*, 357–360. <http://doi.org/10.1038/nmeth.3317>
- Lazarov, T., Juarez-Carreño, S., Cox, N., & Geissmann, F. (2023). Physiology and diseases of tissue-resident macrophages. *Nature*, *618*, 698–707. <http://doi.org/10.1038/s41586-023-06002-x>
- Lee, J. S., Koh, J. Y., Yi, K., Kim, Y. I., Park, S. J., Kim, E. H., Kim, S. M., Park, S. H., Ju, Y. S., Choi, Y. K., & Park, S. H. (2021). Single-cell transcriptome of bronchoalveolar lavage fluid reveals sequential change of macrophages during SARS-CoV-2 infection in ferrets. *Nature Communications*, *12*, 4567. <http://doi.org/10.1038/s41467-021-24807-0>
- Li, F., Piattini, E., Pohlmeier, L., Feng, Q., Rehrauer, H., & Kopf, M. (2022). Monocyte-derived alveolar macrophages autonomously determine severe outcome of respiratory viral infection. *Science Immunology*, *7*, eabj5761. <http://doi.org/10.1126/sciimmunol.abj5761>
- Li, J. T., Melton, A. C., Su, G., Hamm, D. E., LaFemina, M., Howard, J., Fang, X., Bhat, S., Huynh, K.-M., O’Kane, C. M., Ingram, R. J., Muir, R. R., McAuley, D. F., Matthay, M. A., & Sheppard, D. (2015). Unexpected role for adaptive $\alpha\beta$ Th17 cells in acute respiratory distress syndrome. *Journal of Immunology (Baltimore, Md.: 1950)*, *195*, 87–95. <http://doi.org/10.4049/jimmunol.1500054>
- Liu, A., Park, J. H., Zhang, X., Sugita, S., Naito, Y., Lee, J. H., Kato, H., Hao, Q., Matthay, M. A., & Lee, J. W. (2019). Therapeutic effects of hyaluronic acid in bacterial pneumonia in perfused human lungs. *American Journal of Respiratory and Critical Care Medicine*, *200*, 1234–1245. <http://doi.org/10.1164/rccm.201812-2296OC>
- Mass, E., Nimmerjahn, F., Kierdorf, K., & Schlitzer, A. (2023). Tissue-specific macrophages: How they develop and choreograph tissue biology. *Nature Reviews Immunology*, *23*, 563–579. <http://doi.org/10.1038/s41577-023-00848-y>
- Matthay, M. A., Zemans, R. L., Zimmerman, G. A., Arabi, Y. M., Beitler, J. R., Mercat, A., Herridge, M., Randolph, A. G., & Calfee, C. S. (2019). Acute respiratory distress syndrome. *Nature Reviews Disease Primers*, *5*, 18. <http://doi.org/10.1038/s41572-019-0069-0>
- Mould, K. J., Barthel, L., Mohning, M. P., Thomas, S. M., McCubbrey, A. L., Danhorn, T., Leach, S. M., Fingerlin, T. E., O’Connor, B. P., Reisz, J. A., D’Alessandro, A., Bratton, D. L., Jakubzick, C. V., & Janssen, W. J. (2017). Cell origin dictates programming of resident versus recruited macrophages during acute lung injury. *American Journal of Respiratory Cell and Molecular Biology*, *57*, 294–306. <http://doi.org/10.1165/rcmb.2017-0061OC>
- O’Brien, K., Breyne, K., Ughetto, S., Laurent, L. C., & Breakefield, X. O. (2020). RNA delivery by extracellular vesicles in mammalian cells and its applications. *Nature Reviews Molecular Cell Biology*, *21*, 585–606. <http://doi.org/10.1038/s41580-020-0251-y>
- Park, M. D., Silvin, A., Ginhoux, F., & Merad, M. (2022). Macrophages in health and disease. *Cell*, *185*, 4259–4279. <http://doi.org/10.1016/j.cell.2022.10.007>
- Ranieri, V. M., Rubenfeld, G. D., Thompson, B. T., Ferguson, N. D., Caldwell, E., Fan, E., Camporota, L., & Slutsky, A. S. (2012). Acute respiratory distress syndrome: The Berlin definition. *Jama*, *307*, 2526–2533. <http://doi.org/10.1001/jama.2012.5669>
- Rittirsch, D., Huber-Lang, M. S., Flierl, M. A., & Ward, P. A. (2009). Immunodesign of experimental sepsis by cecal ligation and puncture. *Nature Protocols*, *4*, 31–36. <http://doi.org/10.1038/nprot.2008.214>
- Ross, E. A., Douglas, M. R., Wong, S. H., Ross, E. J., Curnow, S. J., Nash, G. B., Rainger, E., Scheel-Toellner, D., Lord, J. M., Salmon, M., & Buckley, C. D. (2006). Interaction between integrin α 9 β 1 and vascular cell adhesion molecule-1 (VCAM-1) inhibits neutrophil apoptosis. *Blood*, *107*, 1178–1183. <http://doi.org/10.1182/blood-2005-07-2692>
- Saravia, J., Chapman, N. M., & Chi, H. (2019). Helper T cell differentiation. *Cellular & Molecular Immunology*, *16*, 634–643. <http://doi.org/10.1038/s41423-019-0220-6>
- Schupp, J. C., Adams, T. S., Cosme, C., Raredon, M. S. B., Yuan, Y., Omote, N., Poli, S., Chioccioli, M., Rose, K. A., Manning, E. P., Sauler, M., DeLuliis, G., Ahangari, F., Neumark, N., Habermann, A. C., Gutierrez, A. J., Bui, L. T., Lafyatis, R., Pierce, R. W., ... Kaminski, N. (2021). Integrated single-cell atlas of endothelial cells of the human lung. *Circulation*, *144*, 286–302. <http://doi.org/10.1161/CIRCULATIONAHA.120.052318>
- Shao, H., Im, H., Castro, C. M., Breakefield, X., Weissleder, R., & Lee, H. (2018). New technologies for analysis of extracellular vesicles. *Chemical Reviews*, *118*, 1917–1950. <http://doi.org/10.1021/acs.chemrev.7b00534>
- Shaw, T. D., McAuley, D. F., & O’Kane, C. M. (2019). Emerging drugs for treating the acute respiratory distress syndrome. *Expert Opinion on Emerging Drugs*, *24*, 29–41. <http://doi.org/10.1080/14728214.2019.1591369>
- Singer, M., Deutschman, C. S., Seymour, C. W., Shankar-Hari, M., Annane, D., Bauer, M., Bellomo, R., Bernard, G. R., Chiche, J.-D., Cooper-Smith, C. M., Hotchkiss, R. S., Levy, M. M., Marshall, J. C., Martin, G. S., Opal, S. M., Rubenfeld, G. D., van der Poll, T., Vincent, J.-L., & Angus, D. C. (2016). The third international consensus definitions for sepsis and septic shock (Sepsis-3). *Jama*, *315*, 801–810. <http://doi.org/10.1001/jama.2016.0287>
- Sorkin, M., Huber, A. K., Hwang, C., Carson, W. F., Menon, R., Li, J., Vasquez, K., Pagani, C., Patel, N., Li, S., Visser, N. D., Niknafs, Y., Loder, S., Scola, M., Nycz, D., Gallagher, K., McCauley, L. K., Xu, J., James, A. W., ... Levi, B. (2020). Regulation of heterotopic ossification by monocytes in a mouse model of aberrant wound healing. *Nature Communications*, *11*, 722. <http://doi.org/10.1038/s41467-019-14172-4>
- Thompson, B. T., Chambers, R. C., & Liu, K. D. (2017). Acute respiratory distress syndrome. *The New England Journal of Medicine*, *377*, 562–572. <http://doi.org/10.1056/NEJMra1608077>
- Urabe, F., Patil, K., Ramm, G. A., Ochiya, T., & Soekmadji, C. (2021). Extracellular vesicles in the development of organ-specific metastasis. *Journal of Extracellular Vesicles*, *10*, e12125. <http://doi.org/10.1002/jev2.12125>
- van Niel, G., Carter, D. R. F., Clayton, A., Lambert, D. W., Raposo, G., & Vader, P. (2022). Challenges and directions in studying cell-cell communication by extracellular vesicles. *Nature Reviews Molecular Cell Biology*, *23*, 369–382. <http://doi.org/10.1038/s41580-022-00460-3>
- van Niel, G., D’Angelo, G., & Raposo, G. (2018). Shedding light on the cell biology of extracellular vesicles. *Nature Reviews Molecular Cell Biology*, *19*, 213–228. <http://doi.org/10.1038/nrm.2017.125>
- Xu, J., Wang, J., Wang, X., Tan, R., Qi, X., Liu, Z., Qu, H., Pan, T., Zhan, Q., Zuo, Y., Yang, W., & Liu, J. (2020). Soluble PD-L1 improved direct ARDS by reducing monocyte-derived macrophages. *Cell Death & Disease*, *11*, 934. <http://doi.org/10.1038/s41419-020-03139-9>
- Xue, M., Xie, J., Liu, L., Huang, Y., Guo, F., Xu, J., Yang, Y., & Qiu, H. (2019). Early and dynamic alterations of Th2/Th1 in previously immunocompetent patients with community-acquired severe sepsis: A prospective observational study. *Journal of Translational Medicine*, *17*, 57. <http://doi.org/10.1186/s12967-019-1811-9>
- Yamashita, T., Iwakura, T., Matsui, K., Kawaguchi, H., Obana, M., Hayama, A., Maeda, M., Izumi, Y., Komuro, I., Ohsugi, Y., Fujimoto, M., Naka, T., Kishimoto, T., Nakayama, H., & Fujio, Y. (2011). IL-6-mediated Th17 differentiation through ROR γ t is essential for the initiation of experimental autoimmune myocarditis. *Cardiovascular Research*, *91*, 640–648. <http://doi.org/10.1093/cvr/cvr148>
- Yates, A. G., Pink, R. C., Erdbrügger, U., Siljander, P. R. M., Dellar, E. R., Pantazi, P., Akbar, N., Cooke, W. R., Vatish, M., Dias-Neto, E., Anthony, D. C., & Couch, Y. (2022). In sickness and in health: The functional role of extracellular vesicles in physiology and pathology in vivo: Part II: Pathology: Part II: Pathology. *Journal of Extracellular Vesicles*, *11*, e12190. <http://doi.org/10.1002/jev2.12190>
- Yu, H., Lin, L., Zhang, Z., Zhang, H., & Hu, H. (2020). Targeting NF- κ B pathway for the therapy of diseases: Mechanism and clinical study. *Signal Transduction and Targeted Therapy*, *5*, 209. <http://doi.org/10.1038/s41392-020-00312-6>
- Yu, Z. X., Ji, M. S., Yan, J., Cai, Y., Liu, J., Yang, H. F., Li, Y., Jin, Z. C., & Zheng, J. X. (2015). The ratio of Th17/Treg cells as a risk indicator in early acute respiratory distress syndrome. *Critical Care (London, England)*, *19*, 82. <http://doi.org/10.1186/s13054-015-0811-2>

SUPPORTING INFORMATION

Additional supporting information can be found online in the Supporting Information section at the end of this article.

How to cite this article: Wang, L., Tang, Y., Tang, J., Liu, X., Zi, S., Li, S., Chen, H., Liu, A., Huang, W., Xie, J., Liu, L., Chao, J., & Qiu, H. (2024). Endothelial cell-derived extracellular vesicles expressing surface VCAM1 promote sepsis-related acute lung injury by targeting and reprogramming monocytes. *Journal of Extracellular Vesicles*, 13, e12423. <https://doi.org/10.1002/jev2.12423>